USAFSAM-TR-87-13

AD-A202 907

ACCURATE DETERMINATION OF THE COMPLEX PERMITTIVITY OF BIOLOGICAL TISSUE AROUND 35 GHz

Rodney J. Sheppard, Ph.D.

Physics Department
King's College, London
Strand, London WC2R 2LS, UK

September 1988

DTIC
ELECTE
17 JAN 1989
S
E
D

Final Report for Period 15 March 1984 - 14 March 1986
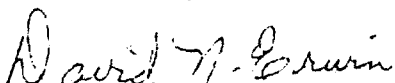
89 1 17 220

NOTICES

This final report was submitted by the Physics Department, King's College, Strand, London WC2R 2LS, United Kingdom, under contract AFOSR-84-0097, job order 2312-W1-07, with the USAF School of Aerospace Medicine, Human Systems Division, AFSC, Brooks Air Force Base, Texas. Dr David N. Erwin (USAFSAM/RZP) was the Laboratory Project Scientist-in-Charge.

When Government drawings, specifications, or other data are used for any purpose other than in connection with a definitely Government-related procurement, the United States Government incurs no responsibility nor any obligation whatsoever. The fact that the Government may have formulated or in any way supplied the said drawings, specifications, or other data, is not to be regarded by implication, or otherwise in any manner construed, as licensing the holder, or any other person or corporation; or as conveying any rights or permission to manufacture, use, or sell any patented invention that may in any way be related thereto.

The animals involved in this study were procured, maintained, and used in accordance with the Animal Welfare Act and the "Guide for the Care and Use of Laboratory Animals" prepared by the Institute of Laboratory Animal Resources - National Research Council.

The Office of Public Affairs has reviewed this report, and it is releasable to the National Technical Information Service, where it will be available to the general public, including foreign nationals.

This report has been reviewed and is approved for publication.

DAVID N. ERWIN, Ph.D.
Project Scientist

JOHN C. MITCHELL, B.S.
Supervisor

JEFFREY G. DAVIS, Colonel, USAF, MC
Commander

REPORT DOCUMENTATION PAGE	Form Approved OMB No. 0704-0188

1a. REPORT SECURITY CLASSIFICATION Unclassified	1b. RESTRICTIVE MARKINGS

2a. SECURITY CLASSIFICATION AUTHORITY	3. DISTRIBUTION / AVAILABILITY OF REPORT Approved for public release; distribution is unlimited.
2b. DECLASSIFICATION / DOWNGRADING SCHEDULE	

4. PERFORMING ORGANIZATION REPORT NUMBER(S)	5. MONITORING ORGANIZATION REPORT NUMBER(S) USAFSAM-TR-87-13

6a. NAME OF PERFORMING ORGANIZATION Physics Department King's College, London	6b. OFFICE SYMBOL (If applicable)	7a. NAME OF MONITORING ORGANIZATION European Office of Aerospace Research and Development (LSB)
6c. ADDRESS (City, State, and ZIP Code) King's College, Strand, London, WC2R 2LS United Kingdom		7b. ADDRESS (City, State, and ZIP Code) 223/231 Old Marylebone Road London, NW1 5th, United Kingdom

8a. NAME OF FUNDING / SPONSORING ORGANIZATION USAF School of Aerospace Medicine	8b. OFFICE SYMBOL (If applicable) USAFSAM/RZP	9. PROCUREMENT INSTRUMENT IDENTIFICATION NUMBER Grant AFOSR 84-0097

8c. ADDRESS (City, State, and ZIP Code) Human Systems Division (AFSC) Brooks Air Force Base, TX 78235-5301	10. SOURCE OF FUNDING NUMBERS

PROGRAM ELEMENT NO.	PROJECT NO.	TASK NO	WORK UNIT ACCESSION NO
61102F	2312	W1	07

11. TITLE (Include Security Classification)

Accurate Determination of the Complex Permittivity of Biological Tissue Around 35 GHz

12. PERSONAL AUTHOR(S)
Sheppard, Rodney J.

13a. TYPE OF REPORT Final	13b. TIME COVERED FROM 84/3/15 TO 86/3/14	14. DATE OF REPORT (Year, Month, Day) 1988, September	15. PAGE COUNT 54

16. SUPPLEMENTARY NOTATION

17.	COSATI CODES		18. SUBJECT TERMS (Continue on reverse if necessary and identify by block number)
FIELD	GROUP	SUB-GROUP	complex permittivity, tissues (biology), microwaves, solid tissues, phantom tissue equivalent water, 35 GHz, dielectric properties, P.T.O.
06	07		
20	14		

19. ABSTRACT (Continue on reverse if necessary and identify by block number)

Apparatus is described which enables the complex permittivity of liquids and solid tissue to be measured at a frequency of 35 GHz. The results are presented on various rabbit tissues, including muscle, fat, skin, brain tissues, and eye lens; and some phantom tissue equivalent materials have been devised.

Various liquids have been measured, including rabbit blood, water, and saline. The results have been examined for any evidence of an anomalous/resonant behavior, but none was found.

20. DISTRIBUTION / AVAILABILITY OF ABSTRACT ☒ UNCLASSIFIED/UNLIMITED ☐ SAME AS RPT ☐ DTIC USERS	21 ABSTRACT SECURITY CLASSIFICATION Unclassified
22a. NAME OF RESPONSIBLE INDIVIDUAL David N. Erwin	22b TELEPHONE (Include Area Code) 512/536-3582	22c OFFICE SYMBOL USAFSAM/RZP

DD Form 1473, JUN 86   Previous editions are obsolete.   SECURITY CLASSIFICATION OF THIS PAGE

TABLE OF CONTENTS

QUALITY INSPECTED 2

Availability Codes

Dist	Avail and/or Special
A-1	

List of Figures

List of Tables

ACCURATE DETERMINATION OF THE COMPLEX PERMITTIVITY
OF BIOLOGICAL TISSUE AROUND 35 GHz

1. INTRODUCTION

During 1981 to 1984, a research program was undertaken for the U.S. Air Force to set up precision coaxial line apparatus to measure the complex permittivity of solid tissues over the frequency range of 1 to 18 GHz.

This final report details the next phase of the work which is to extend the measurement capability to 35 GHz. A new automated waveguide system, with on-line computer control, has been designed and built for the accurate measurement of the complex permittivity of liquids and tissues at 35 GHz. Test data on the new system are presented and followed by measurements on a range of liquids and tissues. The tissue data have been examined carefully for any evidence of anomalous (i.e., resonance) behavior, but none was found.

2. BACKGROUND TO THE WORK

Apart from some pioneering work, such as Schwan[1] very few data concerning the electrical properties of tissues have appeared in the literature until recent times. However, within the past decade numerous papers have been published and many tissues are now well covered; to cite but a few papers.[2,3,4,5] Almost all of the experimental systems described in the literature and the data presented cover frequencies less than 20 GHz. I have contributed to such work;[6,7,8,9] the investigation being supported from 1981 to 1984 by the U.S. Air Force under grant AFOSR-81-0097.

To consider systems to measure the complex permittivity of tissues above 20 GHz, there is the broad-band system developed by Gandhi.[10,11] The paucity of high-frequency data is confirmed by Toler[12] who, as part of a report for the U.S. Air Force, surveyed the literature available on tissues, and cited only the limited data of Edrich and Hardee[13] in the 40- to 90-GHz band. However, it is believed that the almost total lack of permittivity data on tissues at frequencies above 20 GHz is not due to lack of interest but rather the technical difficulty and expense associated with the experimentation.

Apart from the obvious desire for data at the higher microwave frequencies, it has been suggested that this data may cover a region of particular interest and that some biological systems may exhibit an anomalous behavior. In particular, the theoretician Frohlich[14,15] has considered that resonances

are likely to occur. Such resonances have been suggested in the studies concerning the effect of microwaves on the rate of growth of yeast cells.[16,17] Davis and coworkers[18] have reported anomalies in the dielectric dispersion of deoxyribonucleic acid (DNA) at frequencies even less than 10 GHz.

However, some reservations have been expressed concerning such anomalous effects. For example, at the 1985 Bioelectromagnetics Society Meeting, Gandhi and coworkers[19] reported that although the experiments of Grundler and Keilmann had been repeated, the anomalous effects had not been replicated concerning DNA resonances; again attempts to observe the reported anomalies of Davis and coworkers have not been successful. Measurements have been made in our laboratory on a DNA sample provided by Davis; resonances were not seen although a later analysis of the sample did show some deterioration.

The lack of reliable permittivity data on tissues above 20 GHz, coupled with the importance of the frequency region and the controversy surrounding some published data, led to a desire to undertake the present project. The purpose of the work was to devise and set up an experimental system which would enable complex permittivity to be measured, with precision, at 35 GHz. Although the main objective was to study tissues, it was realized that a flexible system which could also measure liquids would be the most valuable. Thus, the main purpose of the project was to make accurate measurements, at 35 GHz, of the complex permittivity of biological systems, with particular reference to tissues. Although it was not a direct objective to look for possible resonances, the data obtained have been studied carefully to see whether there is any evidence of an anomalous behavior.

3. PRELIMINARY CONSIDERATIONS

In conjunction with Professor E. H. Grant, I had already designed a system to measure tissues up to 18 GHz;[6,20] the system being a development of the classic Von Hippel technique. A proposal was made to use the same method at 35 GHz, using waveguide rather than coaxial lines; however, a problem immediately became apparent concerning the size of tissue sample required. The 18-GHz system requires, for optimum performance, a sample which is one-quarter wavelength thick ($\lambda/4$) and this sample is about 0.5 mm at 35 GHz. The technique, in essence, measures the phase and amplitude changes, produced in the transmission line, when the sample is inserted, and the complex permittivity $\epsilon = \epsilon' - i\epsilon''$ is calculated from the data. However, ϵ is related to the thickness via a square so that an $\epsilon\%$ error in the sample thickness gives $2\epsilon\%$ error in permittivity. This fact caused concern in the initial stages of the project since it was not known whether a real tissue sample in the order of 0.5-mm thick could be cut and measured to the required accuracy.

Before final decisions were made concerning the new system, and, in particular, before waveguide components were purchased, the theory of existing methods had to be reconsidered with particular reference to the sample thickness.

3.1 Theory - Preliminary Considerations

A system was considered which consisted of the sample, with a polytetra-fluoroethylene (PTFE) block on either side of it and a short circuit placed at a distance x behind one of the blocks (Fig. 1). The previous 1- to 18-GHz system had a fixed short circuit, but in the present case the effect of a moving short circuit is considered. Note, however, that the short circuit is moving in air behind the sample, it does not imply that the sample thickness is varied.

In the following equations, γ_s, γ_p, and γ_a are the propagation constants of the sample, PTFE and air of thickness ds, dp, and da respectively. Note that the complex permittivity of the sample can be derived from propagation constant γ_s using the usual equation for the dominant TE_{10} mode, namely:

$$\epsilon = \frac{c}{2\pi f} (k^2 - \gamma_s^2) \tag{1a}$$

where $\epsilon = \epsilon' - i\epsilon''$ is the complex permittivity

c is the velocity of light

f is the frequency

and $k = [\pi/a]$ where a is the breadth of the waveguide.

The reflection coefficient r_{mn} at the boundary between two media of propagation constants γ_m and γ_n is given by:

$$r_{mn} = \frac{\gamma_m - \gamma_n}{\gamma_m + \gamma_n} \tag{1b}$$

From Figure 1, using the usual equations for multiple reflections, the effective reflection coefficients can be expressed as:

$$r_{56}' = -1 \tag{2}$$

$$r_{45}' = \frac{r_{45} - e^{-2\gamma_a x}}{1 - r_{45}e^{-2\gamma_a x}} \tag{3}$$

3

$$r'_{34} = \frac{r_{34} + r'_{45}e^{-2\gamma_p d_p}}{1 + r_{34}r'_{45}e^{-2\gamma_p d_p}} \qquad (4)$$

In this case, since medium 4 is identical to medium 2.

$$r_{34} = -r_{23}$$

$$r'_{34} = \frac{-r_{23} + r'_{45}e^{-2\gamma_p d_p}}{1 - r_{23}r'_{45}e^{-2\gamma_p d_p}} \qquad (5)$$

$$r'_{23} = \frac{r_{23} + r'_{34}e^{-2\gamma_s d_s}}{1 + r_{23}r'_{34}e^{-2\gamma_s d_s}} \qquad (6)$$

$$r'_{12} = \frac{r_{12} + r'_{23}e^{-2\gamma_p d_p}}{1 + r_{12}r'_{23}e^{-2\gamma_p d_p}} \qquad (7)$$

Thus, the potential difference across the detector is given by

$$V(x) = A|r'_{12}|^n \qquad (8)$$

where A is a constant and n is the characteristic of the detector crystal. Note that for square law behavior n would be equal to 2, but detectors tend not to be exactly square law devices and this behavior is being allowed for by the parameter n.

The important conclusion to be drawn from this work is that from equation (8) r'_{12} is a function of r'_{23} which from equation (6) is a function of the sample thickness ds. Thus, it appears from equation (8) that by measuring the detector voltage V(x) as a function of the short circuit position x it might be possible to obtain the sample thickness d_s during the fitting procedure. However, the inclusion of a parameter in an equation does not imply that accurate and unique information can be obtained on the parameter; this information is considered in the following section.
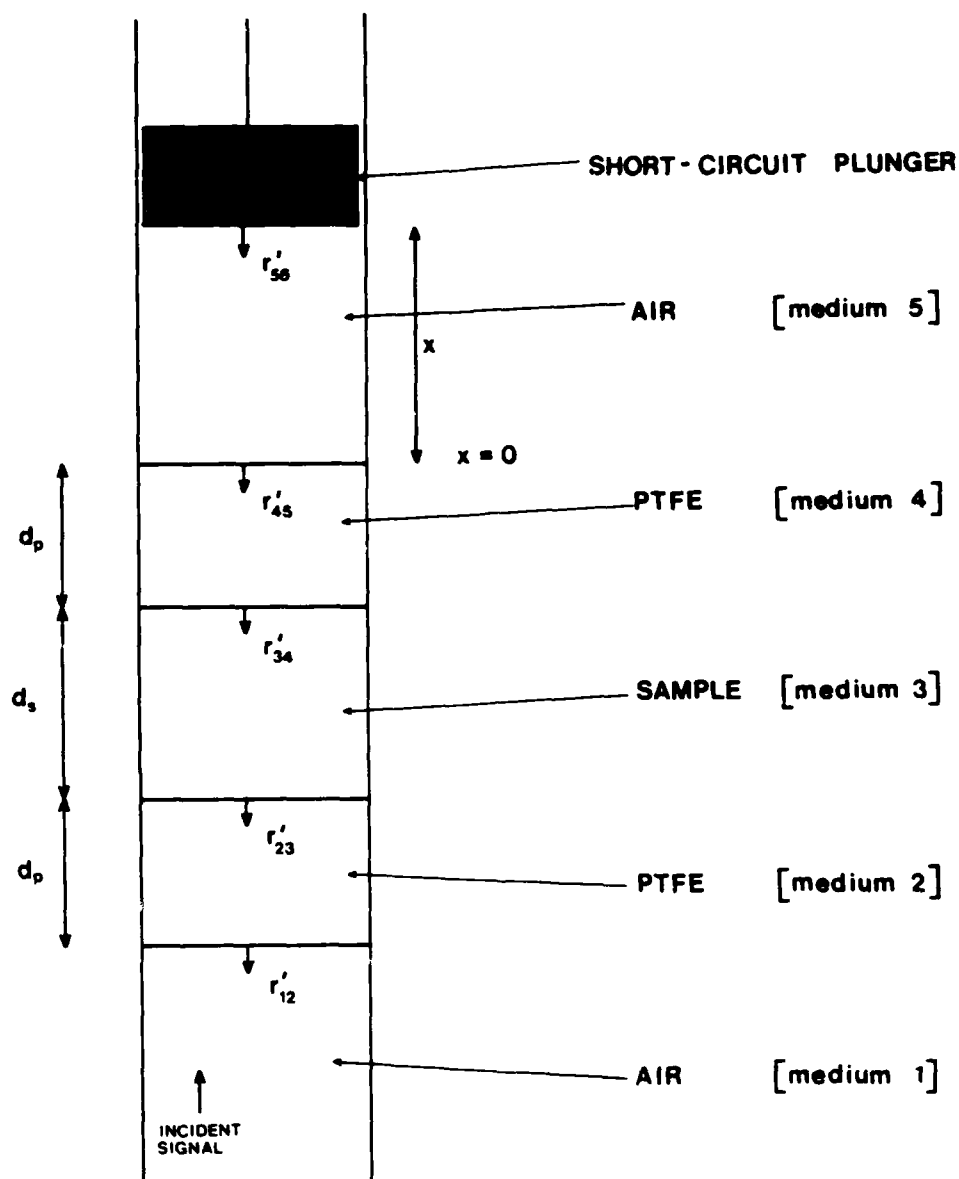
r_{12}' is the effective reflection coefficient of the entire system of interfaces

Figure 1. Schematic representation of tissue sample cell and short-circuit plunger, showing the effective reflection coefficient at each dielectric boundary.

3.2 Simulated Data

The first requirement was to ensure that variations in the complex permittivity could be "seen" in the data. Values of permittivity for water, rabbit brain, and eye lens (obtained from the previous project) over the range 7.5 to 18 GHz were fitted to a Cole-Cole equation. From the parameters obtained, the complex permittivities were estimated at 35 GHz; the results are given in Table 1. Using equation (8), coupled with the other equations on which it depends, reflection profiles were generated and these are shown in Figure 2; there are significant differences between the profiles.

Although these curves suggest that good accuracy could be obtained for the permittivity, it is still necessary to demonstrate and to determine whether the sample thickness ds can be obtained during the least squares curve fitting. To simulate a real situation, typical random noise and systematic errors were added to the generated data. These data were then fitted, a five parameter model being used, containing the parameters ε', ε'' (complex permittivity), ds (sample thickness), Δx (a phase constant) and A (an amplitude constant). The results are shown in Table 2; the first fit is for perfect data without error and as expected the correct parameters are obtained with 0 root mean square (RMSE). For fit 2, the sample thickness was clamped at 0.49 mm instead of the correct value of 0.5 mm and the RMSE is relatively large and ε' and ε'' fit to incorrect values. This result certainly suggests that the data are sensitive to ds as required. In fit 3, the real situation is simulated, errors were added, the phase is offset by 0.1 mm, and all parameters are fitted. The RMSE is reduced to 0.0095; ε' and ε'' together with their 95% confidence intervals cover the true value; and ds is obtained with an error of $\pm$ 0.003 mm. These results clearly demonstrate that not only can the sample thickness be obtained during the fitting procedure, but it can be obtained to a high degree of precision.

3.3 Preliminary Conclusions

The work just mentioned shows that, if required, the thickness of a tissue sample could be determined during the data analysis. For maximum accuracy, a slotted line would be included in the circuit; thus, at each short circuit position the slotted line's probe would be moved and the standing wave profile recorded. However, this procedure would be lengthy, even if the slotted line and short circuit movements were automated.

Thus, a decision was made to set up a system based upon that used at 18 GHz and to assess the accuracy for tissues using a fixed short circuit which would enable rapid data acquisition. However, the system was designed so that a moving short circuit could be used, if experience showed it to be required. Definitely, a moving short circuit is needed for precision data on liquids.

TABLE 1.   THE COMPLEX PERMITTIVITY AT 35 GHz, ESTIMATED FROM
LOWER FREQUENCY DATA

Substance	ϵ'	ϵ''
Water	19.5	29.1
Rabbit Brain	13.6	14
Rabbit Eye Lens	10	7.7

TABLE 2.   TO ILLUSTRATE THAT THE SAMPLE THICKNESS CAN BE
FITTED AS A PARAMETER

	$\Delta X/mm$	ϵ'	ϵ''	A	RMSE
1	0.500	0	13.6	14.0	10.0	0.0000
2	0.490	0 ±0.02	13.82 ±0.07	14.21 ±0.14	10.00 ±0.01	0.0297
3	0.501 ±0.004	-0.101 ±0.003	13.56 ±0.18	13.96 ±0.11	10.02 ±0.03	0.0095

Data generated for d_s = 0.5 mm; Δx = 0 mm, in fits 1 and 2 and -0.1 mm in fit 3;
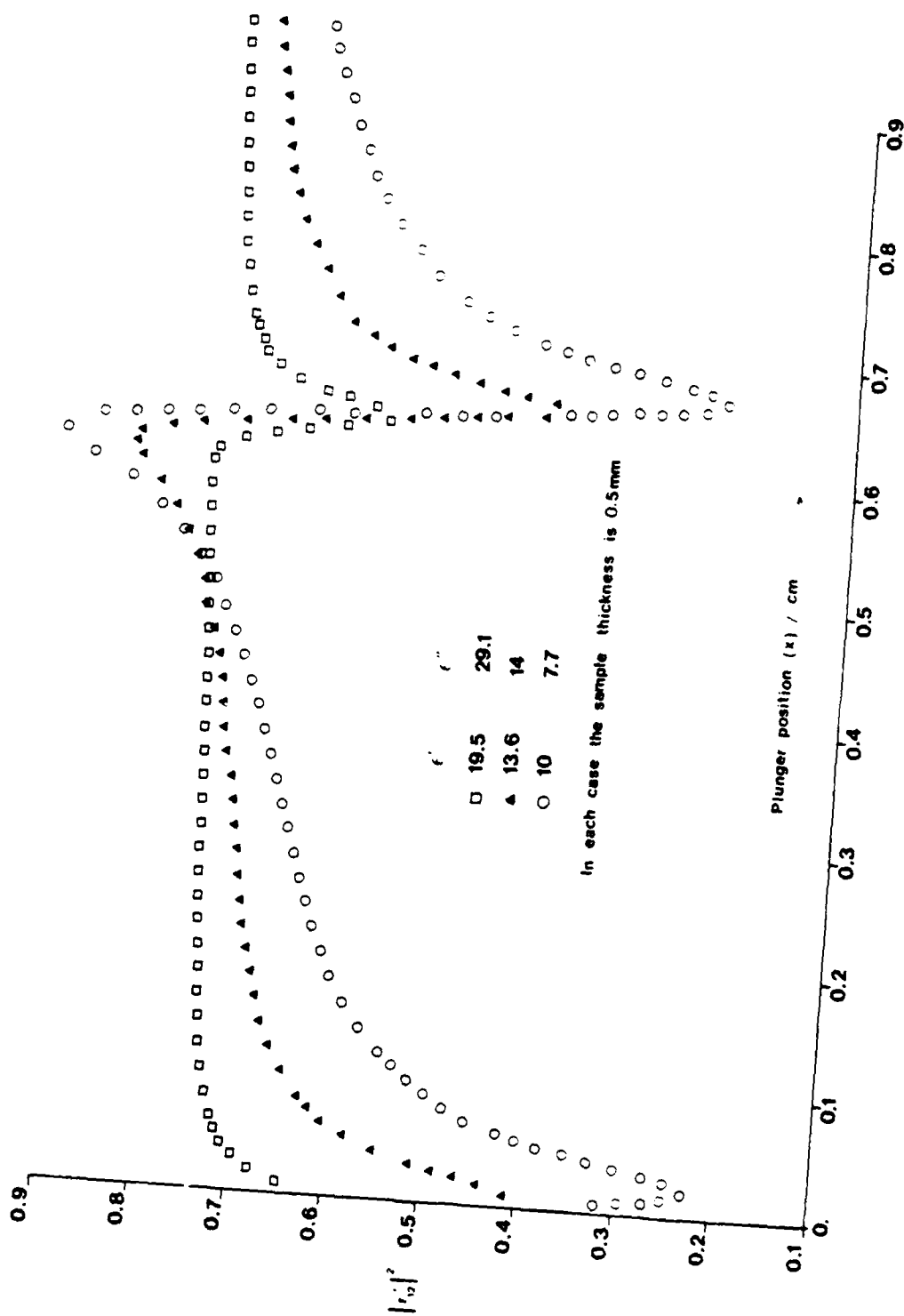ϵ' = 13.6; ϵ'' = 14, A = 10.   All errors are the 95% confidence intervals.

Figure 2. Generated reflection profiles for 3 differing dielectric media.

8

4. GENERAL APPARATUS CONSIDERATIONS

As mentioned earlier, it is necessary to use waveguides, rather than coaxial lines, at 35 GHz and it was decided to use A-band equipment which operates from 26 to 40 GHz. However, in practice the oscillator will have a more limited tuning range and the ferrite components will also restrict the range. In general, the less the bandwidth of certain components, such as ferrites, the better the system performance and for this reason a decision was made to operate at exactly 35 GHz with a minimal tuning range. Since expertise has been gained at 35 GHz, it is believed that good performance could be obtained over a broader band and this confidence forms part of a grant proposal now being funded by AFOSR.

Most of the waveguide components are from the TRG range of Alpha Industries. I have used this American Equipment at 70 GHz for many years and have been satisfied with it.

5. GENERAL THEORY

5.1 Moving Short Circuit - Solids

The theory for this situation has already been considered in Section 3 and equations up to number 8 are the working equations for a short circuit moving behind a <u>fixed</u> (solid) of thickness ds.

5.2 Moving Short Circuits - Liquids

For a moving short circuit, which varies the thickness of a liquid sample, the appropriate equation[22] is

$$P(x) = \left| \frac{R_1 + R_2 \exp(-2\gamma_s x)}{1 + R_3 \exp(-2\gamma_s x)} \right| \tag{9}$$

where R_1, R_2, and R_3 are complex constants which may be calculated during the curve fitting procedure. Power, rather than voltage, is being used for convenience, and x is the relative liquid thickness (variable) and can be measured from any arbitrary point. Thus, as mentioned previously, the complex permittivity $\epsilon = \epsilon' - i\epsilon''$ is related to the propagation constant of the sample γ_s as shown (Eq. 1a) and the curve fitting of equation (9), with ϵ substituted for γ_s, enables ϵ', ϵ'', R_1, R_2, and R_3, together with their 95% confidence intervals, to be obtained.

9

5.3 Fixed Short Circuit - Solids

Although the sample thickness ds is fixed, the probe of a slotted line is moved, where x is the distance of the probe from the PTFE - air interface. As shown in Steel et al.,[6] the working equation is

$$P(x) = |A|^2 |\exp(-\gamma_a x) + r'_{12}\exp(\gamma_a x)|^2 \qquad (10)$$

As mentioned previously, γ_a is the propagation constant of the air filled line, A is a real constant and r'_{12} is the total reflection coefficient of the system. This reflection coefficient is related to the basic parameters of the system in a similar way to those of Section 3, the equations being

$$r'_{12} = \frac{r_{12} + r'_{23}\exp(-2\gamma_p d_p)}{1 + r_{12}r'_{23}\exp(-2\gamma_p d_p)} \qquad (11)$$

$$r'_{23} = \frac{r_{23} - \exp(-2\gamma_p d_p)}{1 - r'_{23}\exp(-2\gamma_s d_s)} \qquad (12)$$

$$r_{12} = \frac{\gamma_a - \gamma_p}{\gamma_a + \gamma_p} \qquad (13)$$

$$r_{23} = \frac{\gamma_p - \gamma_s}{\gamma_p + \gamma_s} \qquad (14)$$

and γ_s is related to ε via equation (1a).

Thus, for all systems either a short circuit or a probe is moved a distance x, and the output power P(x) is measured. The power profile is then recorded as a function of x and a least-squares curve fitting analysis of the data enables parameters of the profile to be obtained, of which two are the complex permittivity $\varepsilon' - i\varepsilon''$. The following section describes the experimental cell and circuit which enables these data to be obtained.

6. APPARATUS - WAVEGUIDE CIRCUIT AND ANCILLARY COMPONENTS

As mentioned previously, A-band (26 to 40 GHz) waveguide apparatus was used; the majority of the equipment was purchased from Alpha Industries. A schematic diagram of the complete system for complex permittivity measurements, at 35 GHz, is shown in Figure 3 and the apparatus is shown in Figure 4.

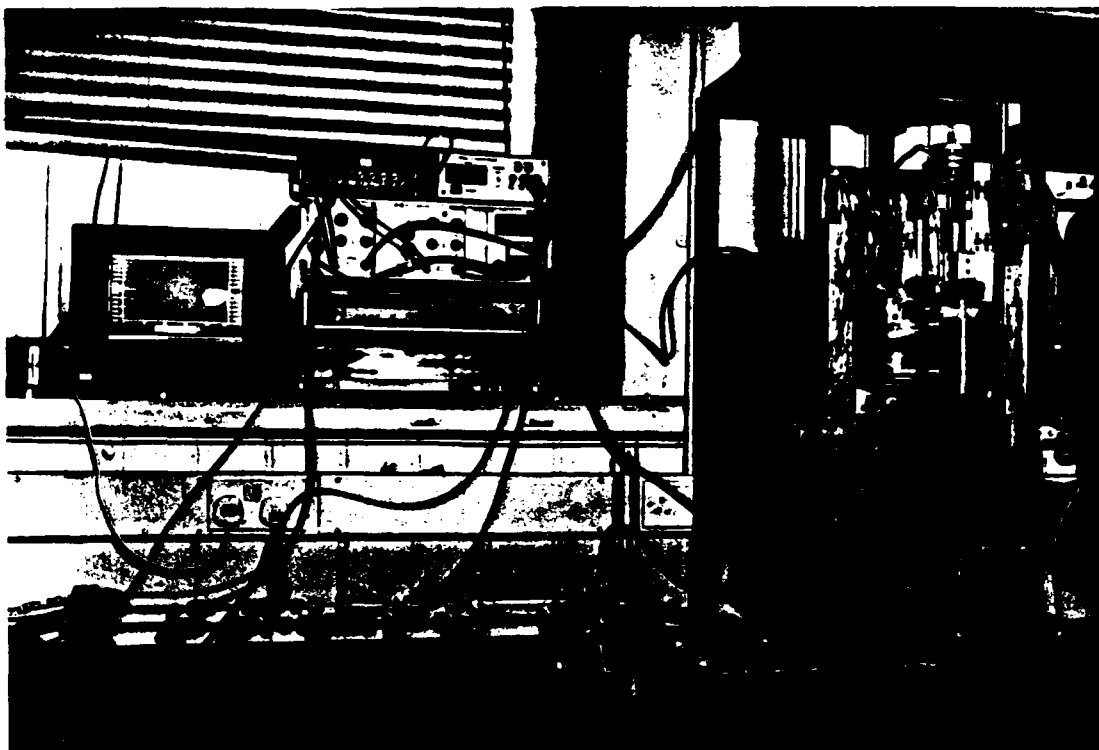Figure 3. A schematic diagram of the 35 GHz apparatus.

Figure 4.   The 35 GHz system.

The system shown is for measuring liquid samples; however, it only requires a change of experimental cell and a minor rearrangement of the components within the dotted region of Figure 3 to enable solid tissues to be studied.

To consider the circuit in detail, 100 mW of continuous-wave power is supplied by a CME720CE Gunn Diode oscillator. To ensure the highest possible stability, particularly before a phase locking frequency counter was available, a water jacket, to surround the oscillator, was designed and built. Thermostatically controlled water is circulated through the jacket to maintain temperature stability of the Gunn Diode; the unit is shown in Figure 5.

The output signal is fed through two 30-dB isolators, via the side arm of a directional coupler into an EIP578 source locking frequency counter. The "fine tune" DC output of the frequency counter is connected directly to the FM input of the Gunn Diode, locking the oscillator frequency at 35 GHz with a stability ±1 Hz. The signal is then modulated at 1 kHz with a ferrite modulator whose driver also triggers a Bentham 223 dual-channel lock-in amplifier to provide synchronous signal detection. The main microwave signal passes through a variable attenuator to a second directional coupler whose side arm consists of a crystal detector preceded by a 30-dB isolator and a variable attenuator. The signal monitor gives an output, V_{mon}, which is proportional to the incident power. A stepping motor controlled rotary vane attenuator varies the power entering the experimental cell and can be used to measure automatically the characteristic of the signal detector diode. The signal then passes through two more 30-dB isolators before entering the experimental sample cell. For liquids, the power reflected from a variable length of sample is detected via a directional coupler. For solids, the standing wave produced from a fixed sample is recorded with the aid of a stepping motor controlled slotted line. In both cases, the detected signal (V_{sig}) is divided by V_{mon} to account for any small fluctuations in oscillator output. The amplified signals from the two detectors are fed from the lock-in amplifier to a scanning unit whose output is connected to a Solartron 7060 digital voltmeter, the system being under the control of a Research Machines 380Z microcomputer and the connections being via an IEEE bus. In practice, it was only necessary to collect four signal and monitor voltages for data averaging, such was the stability of the system. Other devices under computer control (IEEE) include a Keithley 177 digital multimeter which is used to monitor Gunn Diode supply current, the EIP578 frequency counter and two Bentham SMD3B stepping motor drives. The first drive controls a Bentham T300X50 linear translation to accurately move a short circuit plunger through a liquid filled waveguide to a resolution of 0.0025 mm (Fig. 6). However, for solid tissue measurements, this drive controls a Bentham 23/SM stepping motor coupled to a slotted line for automatic reflection coefficient measurements; the probe carriage displacement resolution being 0.03 mm per step. Figure 7 shows the liquid cell (out of use) at the top of the system and the tissue measuring cell and slotted line below. The tissue cell and slotted line are shown in more detail in Figure 8. The second drive unit controls another motor which is coupled to the rotary vane attenuator (Fig. 9). In all cases, the units to hold the stepping motors were

designed as part of the project and built in the Mechanical Workshop of the King's College Physics Department. Plunger and slotted-line probe displacements are measured by Mitutoyo 543-425E digimatic indicators, each having a linear resolution of 0.001 mm, and can be seen in Figures 6, 7, and 8. The digital output of the indicators is converted from binary coded decimal (BCD) to conventional ASCII code by a Mitutoyo MUX-10. These data are then assessed by the microcomputer via the RS232 serial port.

7. EXPERIMENTAL CELLS

As explained in Section 2, it was considered desirable to be able to measure both liquid and solid samples, and this requires more than one experimental cell.

7.1 Cell for Liquid Samples

The experimental cell for measuring the complex permittivity of lossy liquid samples is shown in Figure 10 and can be seen in Figure 6. The cell is a development of that designed by Szwarnowski and Sheppard[23] for use at 70 GHz. However, the thermistor temperature probe has been dispensed with in favor of two thermometers at the inlet and outlet pipes (A) of the stainless steel water jacket (B). This arrangement enables the temperature stability of the liquid sample to be kept to within ±0.05°C. The sample cell is constructed from a length of coin silver WG22 waveguide (C) 7.112 mm by 3.551 mm internal dimensions) with two modified waveguide flanges (D), and a brass collar (E) which facilitates the insertion and attachment of the guide to the water jacket. The cell is secured into position by locking screws (F) and two rubber O-rings (G) prevent the circulating liquid from leaking out of the jacket.

The top of the guide (H) is gently tapered allowing the short circuit (I) to be inserted without damage and the stainless steel reservoir (J) stores excess liquid displaced by the plunger as it moves into the guide. A liquid tight nylon (Polypenco 66) plug (K) holds the sample in the cell and keeps the liquid interface normal to the direction of wave propagation, precluding the generation of higher modes. The noncontacting short circuit is constructed from a block of solid silver (L), 7 mm in length, attached to a 22 mm block of Tufnol (SRBF) (M). The Tufnol has a 0.1 mm groove milled down the long dimension of each side of it and its face is not more than 0.1 mm larger than the silver. This arrangement can be seen in Figure 11 and permits the unrestricted passage of a viscous liquid between the waveguide walls and the plunger, and both insulates the silver from the waveguide walls and acts as a bearing surface for the resulting noncontacting short circuit.
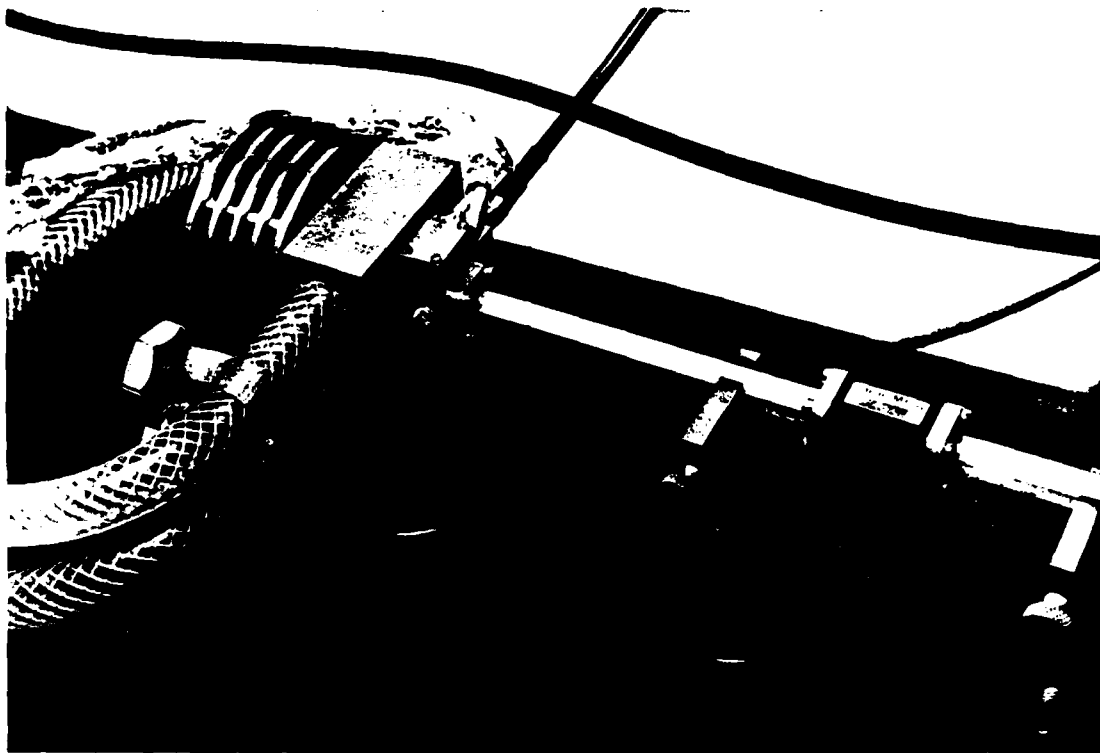
Figure 5.   The Gunn diode and water jacket.
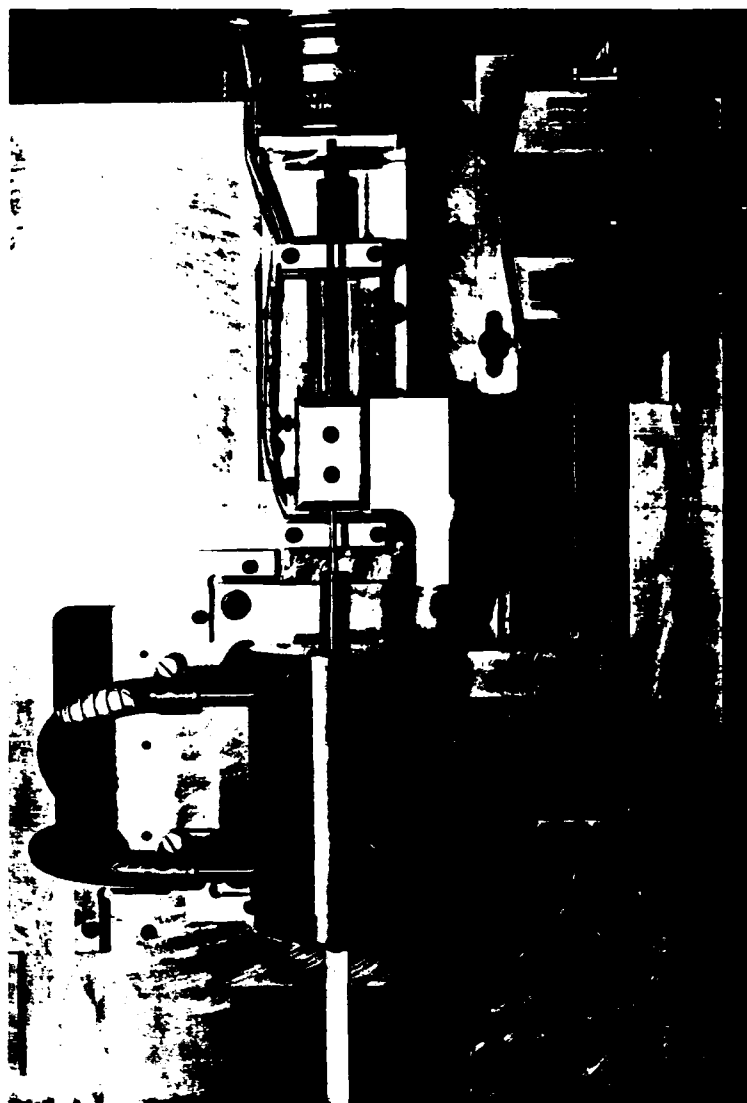
Figure 6. The liquid cell, stepping motor, and digimatic indicator.

Figure 7.   Tissue cell and slotted line--
general arrangement.
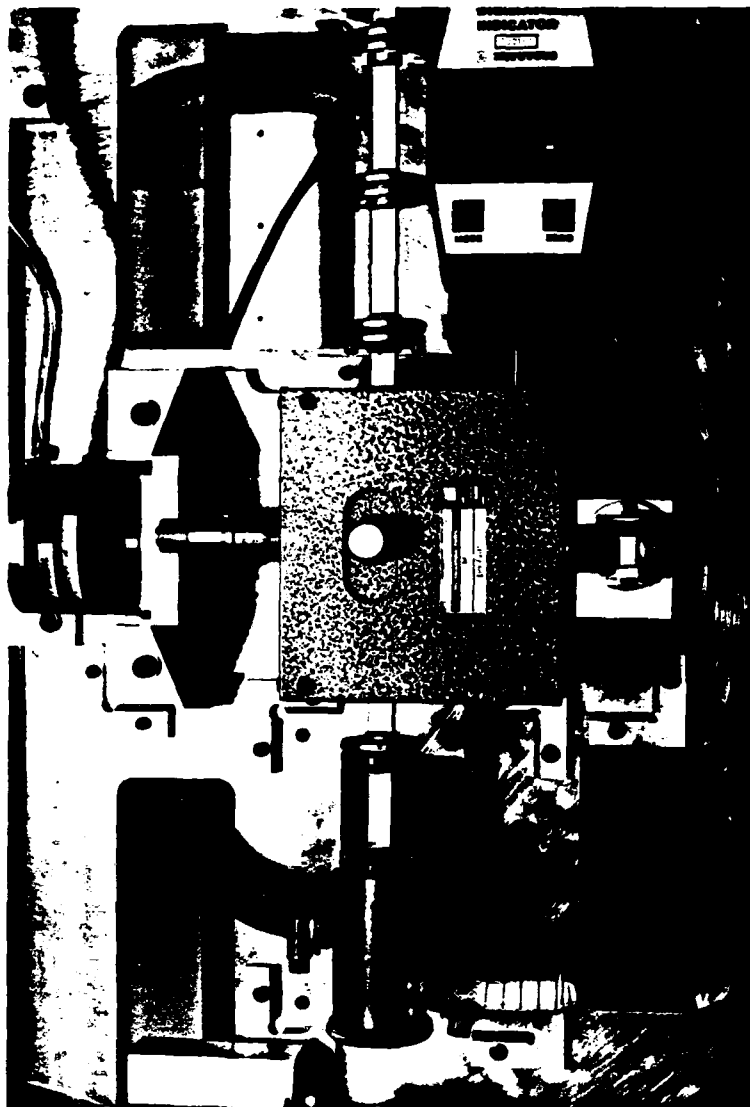
Figure 8. Close-up of the tissue cell and slotted line.
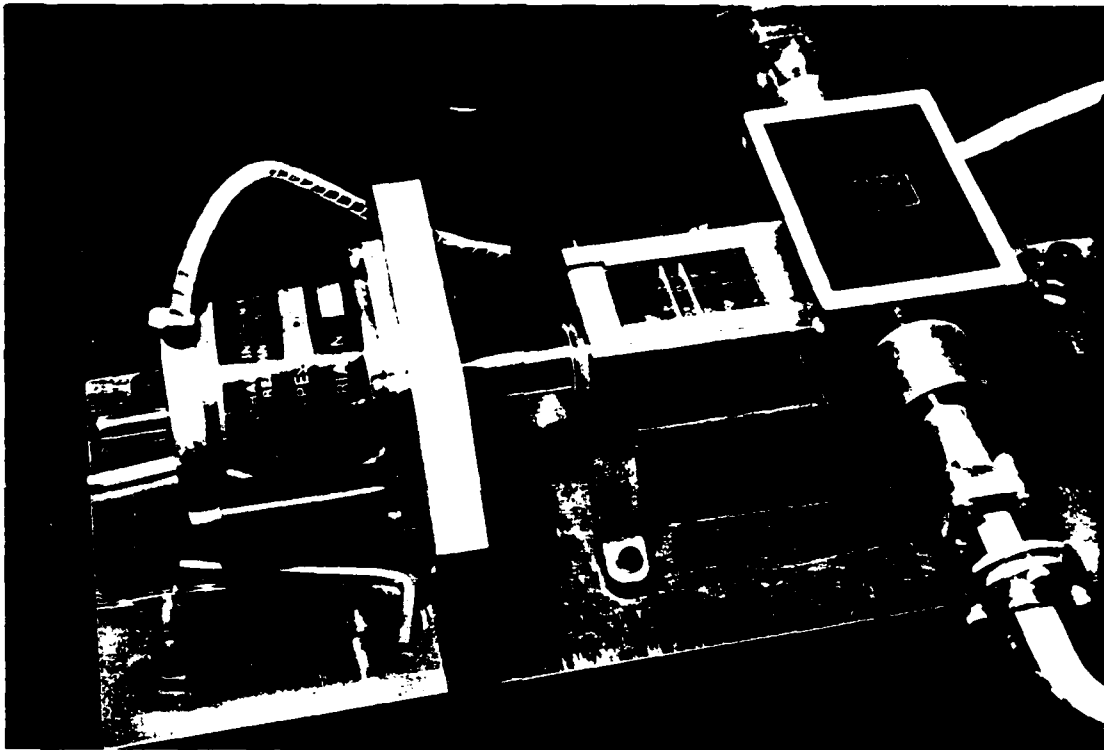
Figure 9. The stepping motor drive for an attenuator.
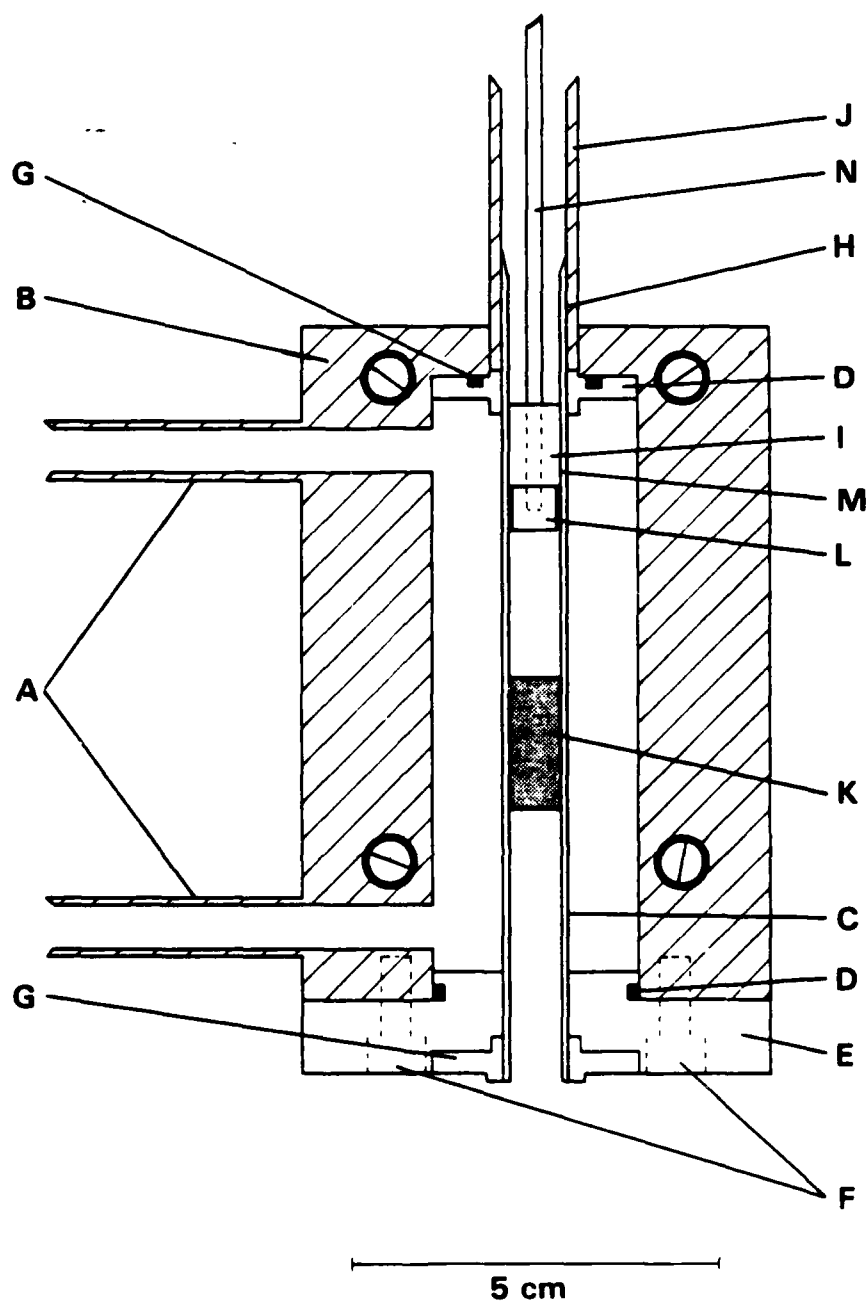
A. Inlet and Outlet Pipes   G. O-Rings   L. Block of Solid Silver
B. Water Jacket   H. Top of Guide   M. Block of Tufnol
C. Waveguide   I. Short Circuit   N. Steel Rod
D. Waveguide Flanges   J. Stainless Steel
E. Brass Collar   Reservoir
F. Locking Screws   K. Nylon Plug

Figure 10.   The experimental cell for measuring a liquid sample.
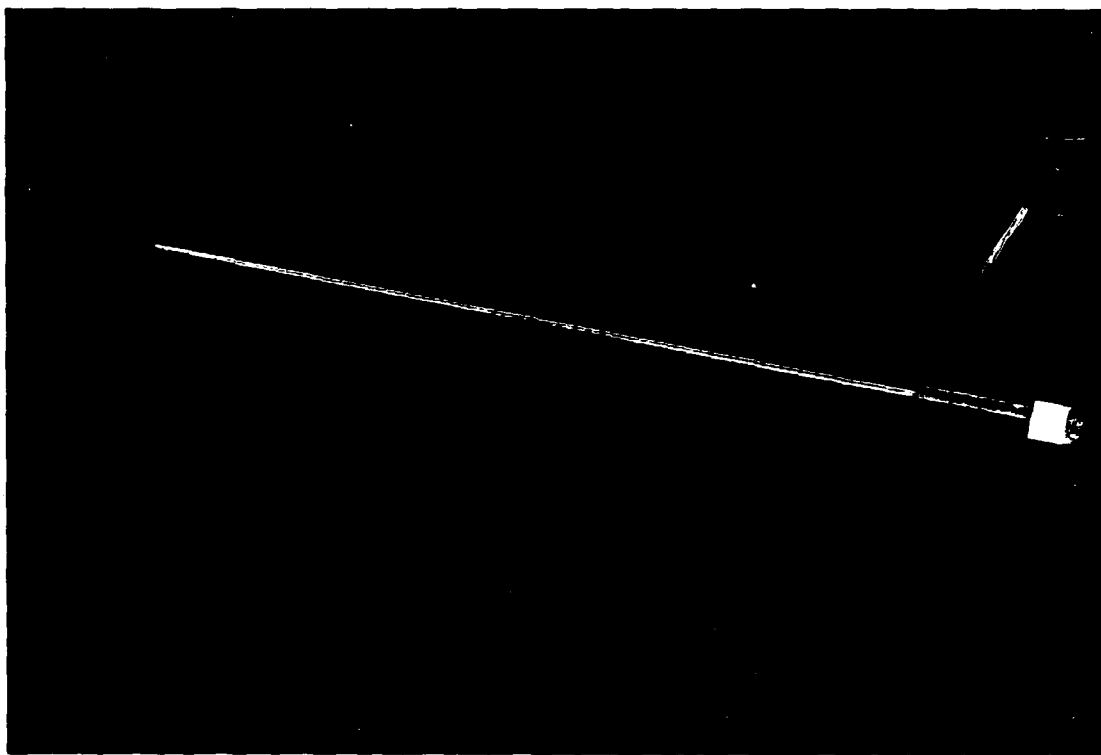
Figure 11. The short circuit.

A steel rod (N) of diameter 2.4 mm passes through the Tufnol and is screwed into the silver block. The other end of the rod is connected to the traveling nut of the linear stage. The contacting type of short circuit described by Szwarnowski and Sneppard[23] was constructed but proved not to be sufficiently versatile. For example, if the required travel needed to exceed 2 mm (for most liquids this was the case), then the contact was not reliable over the total range. It was also found that viscous liquids could not easily pass in or out of the cell.

The short-circuit drive mechanism for the experimental cell is shown in Figures 6 and 12. All of the components are attached to an aluminum baseplate (A), 630 mm in length, 307 mm in width, and 19.3 mm in thickness. The base-plate is mounted on to a tubular rectangular steel frame (B) with the top edge connected to a dead-weight counterbalance (behind the baseplate) via a cable (C) and pulley mechanism permitting height adjustments to be made. The aluminum plate moves on retaining bearings (D) constructed from nylon to reduce friction, and is secured by two locking clamps (E).

The stainless steel shaft (F) from the short circuit is secured by a brass bush embedded within the modified traveling nut (G) of the stepping motor linear stage (H). To keep the linear stage within the bounds of its travel (50 mm maximum), there are protective micro switches at each end. The digimatic indicator (I) is securely attached to the aluminum baseplate in a manner that enables its vertical position to be adjusted. The traveling nut of the linear stage has a staggered lightweight aluminum extension (J) which enables the distance indicator to be positioned next to the linear stage rather than directly above it. This design was preferable under the circumstances, since the indicator is relatively large and to position it above the stage would have required a longer (and heavier) baseplate to accommodate it. Besides, owing to the considerable protrusion of the linear stage, the spindle of the indicator would be approximately 80 mm from the surface of the base-plate, requiring considerable skill to position it vertically with a high degree of mechanical stability. Although this arrangement was found to be unconventional, highly satisfactory results were obtained.

The water jacket surrounding the experimental cell (K) is connected to a smaller aluminum plate (L) by four stainless steel pillars (in Fig. 12 these are obscured by the cell) to improve the thermal isolation between cell and plate; this feature was successfully used previously by Szwarnowski and Sheppard[23] and Nightingale et al.[22] The smaller plate is accurately located on the main baseplate by four aluminum brackets (M) while the other two brackets (N) are for positioning a slotted line and its stepping motor on to the baseplate as required for the solid tissue measurements.
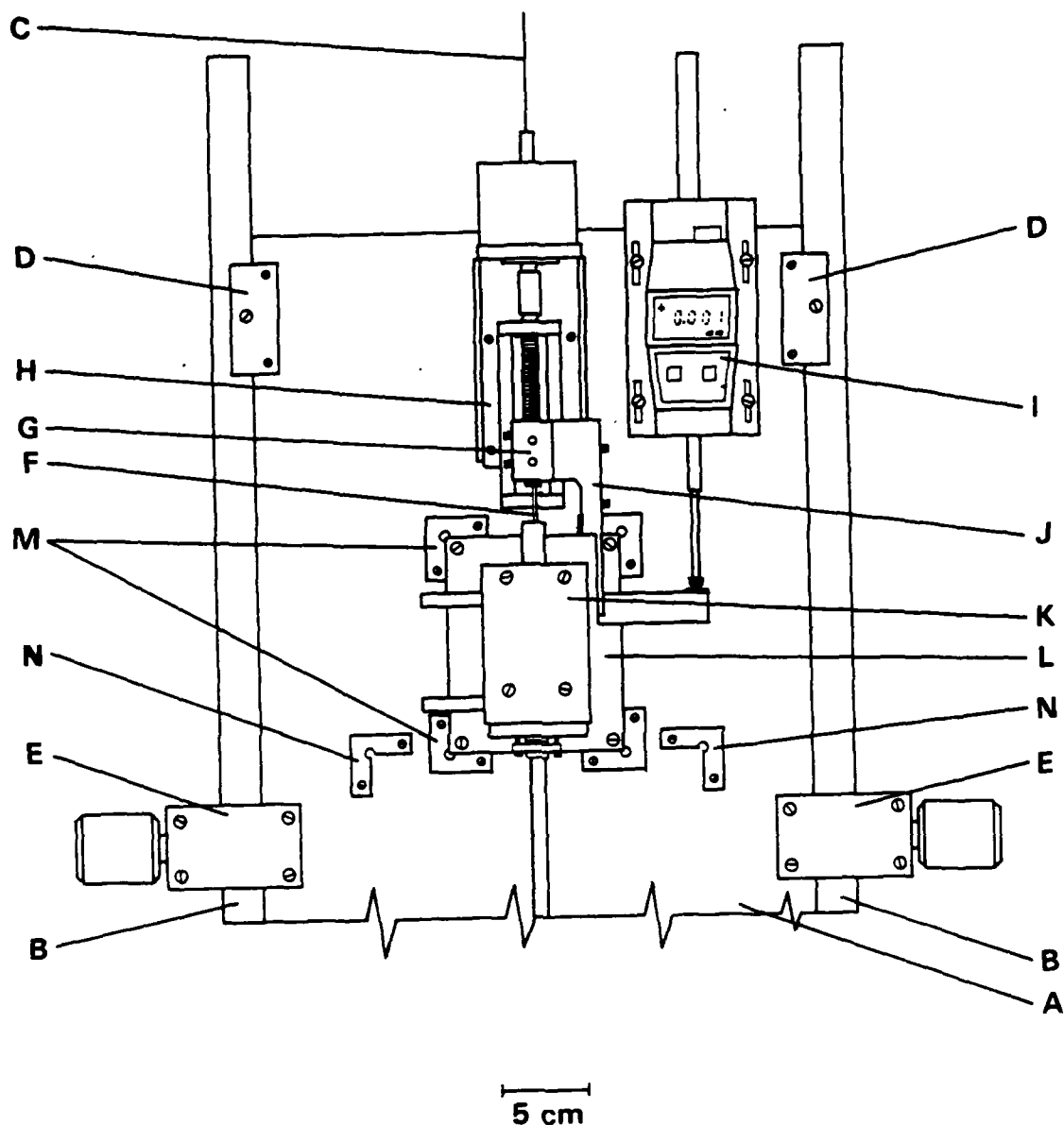
Figure 12. The liquid sample cell and drive mechanism.

A. Aluminum Baseplate
B. Steel Frame
C. Cable
D. Retaining Bearing
E. Locking Clamps

F. Steel Shaft
G. Traveling Nut
H. Motor Linear Stage
I. Digimatic Indicator
J. Aluminum Extension

K. Water Jacket
L. Aluminum Plate
M. Aluminum Brackets
N. Brackets

7.2 Cells for Solid Tissue Samples

In a previous report,[24] a cell was described for solid tissues and consisted of a length of waveguide with a 1 cm long section removed from one of the narrow faces,through which the tissue sample could be loaded (Figs. 13-15). The open section of guide is covered with a brass plate and the whole assembly inserted into a water jacket to thermostat the tissue. The assembly could be mounted onto the baseplate in place of the liquid cell and a moving short circuit introduced into the top of the system.

However, an alternative and simpler cell was also designed and built for measurements with a fixed short circuit (Fig. 16). A cross section of this cell is shown in Figure 17 and comprises a 42 mm straight section of waveguide (A) with flanges at either end (B) and terminated by a fixed brass short circuit (C). The tissue sample (D) resides between the short and a one-half wavelength PTFE plug (E), and is thermostated by a brass water jacket (F) which is secured to the short circuit by two screws (G). A thermistor probe (H) monitors the temperature of the short circuit next to the sample. Around 37°C, the uncertainty of the temperature within the sample is approximately 0.5°C, this error reducing as the measurements approach room temperature. The cell is connected directly to the slotted line and positioned on the main baseplate as described in the previous section.

Although the original cell (Figs. 13 and 14) gave reasonable results, we were worried about the removable brass lid, since no matter how carefully it is made, it does introduce some discontinuity in a very sensitive region. Tests on the cells showed that the system using a fixed short circuit gave adequate accuracy so that the cell of Figure 17 has been used for most of the tissue data presented.

All of the cells just described were built in the mechanical workshop of King's College Physics Department.

8. COMPUTER SOFTWARE

As already mentioned in Section 6, many of the waveguide components are under computer control. In particular, stepping motors have been coupled to the drive of the cells and a variable attenuator, being controlled on-line by a Research Machines 380Z computer via an IEEE-488 bus. A central part of the experimental system is a color visual display unit (Fig. 18), and software has been written so that the status of key instruments and the results as acquired can be displayed. Once a profile is obtained, for example, the voltage output from the lock in amplifier as a function of short-circuit position, it is analyzed by means of least squares curve fitting[25] to obtain the parameters of the profile. In the early stages of the project, the analysis was done on a 380Z computer; however, a Micro VAX II has now been purchased (by non U.S. government funds), and this system has been made available to the project and used for the curve fitting.
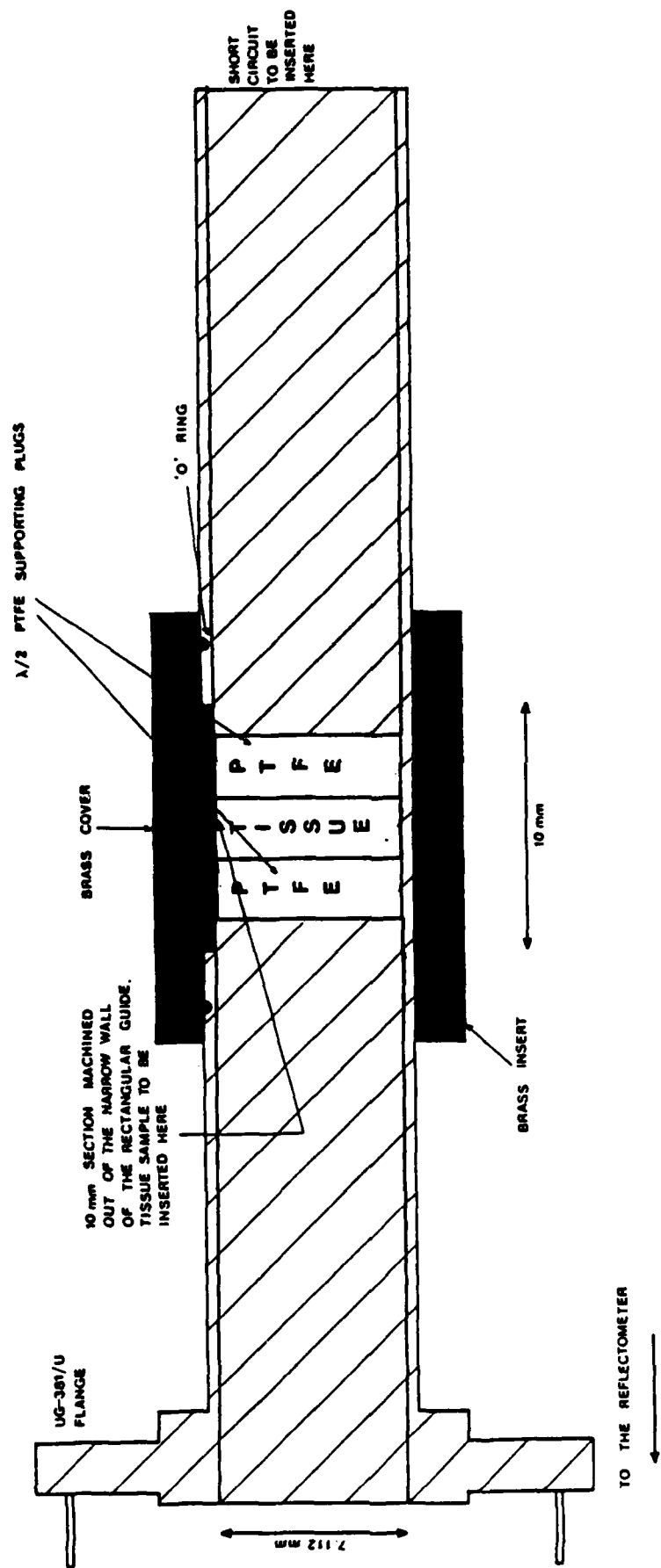
Figure 13. Front section of the waveguide sample cell (35 GHz, A-Band).

25
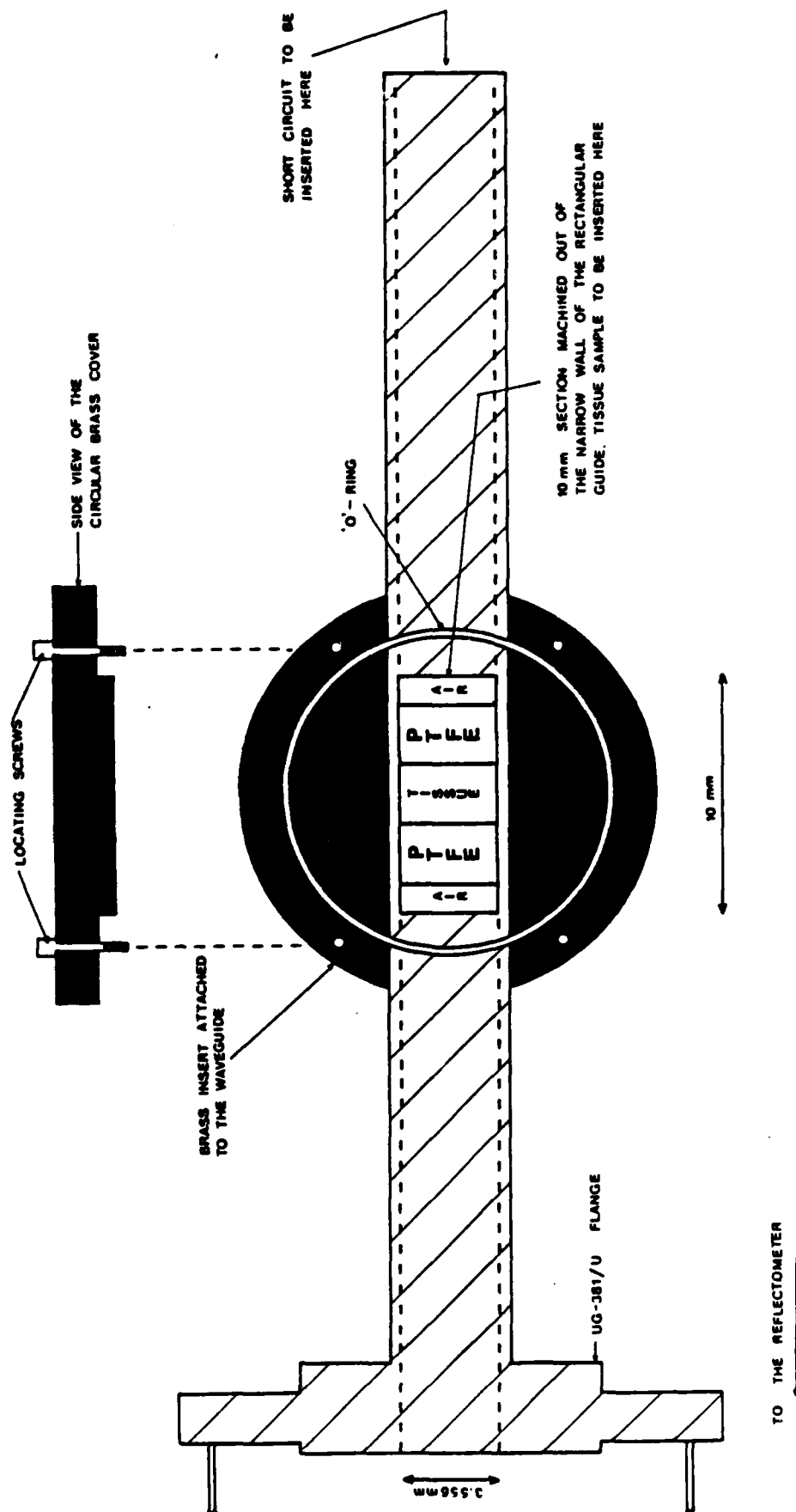
Figure 14. Side view of waveguide tissue sample cell (35 GHz, A-Band).
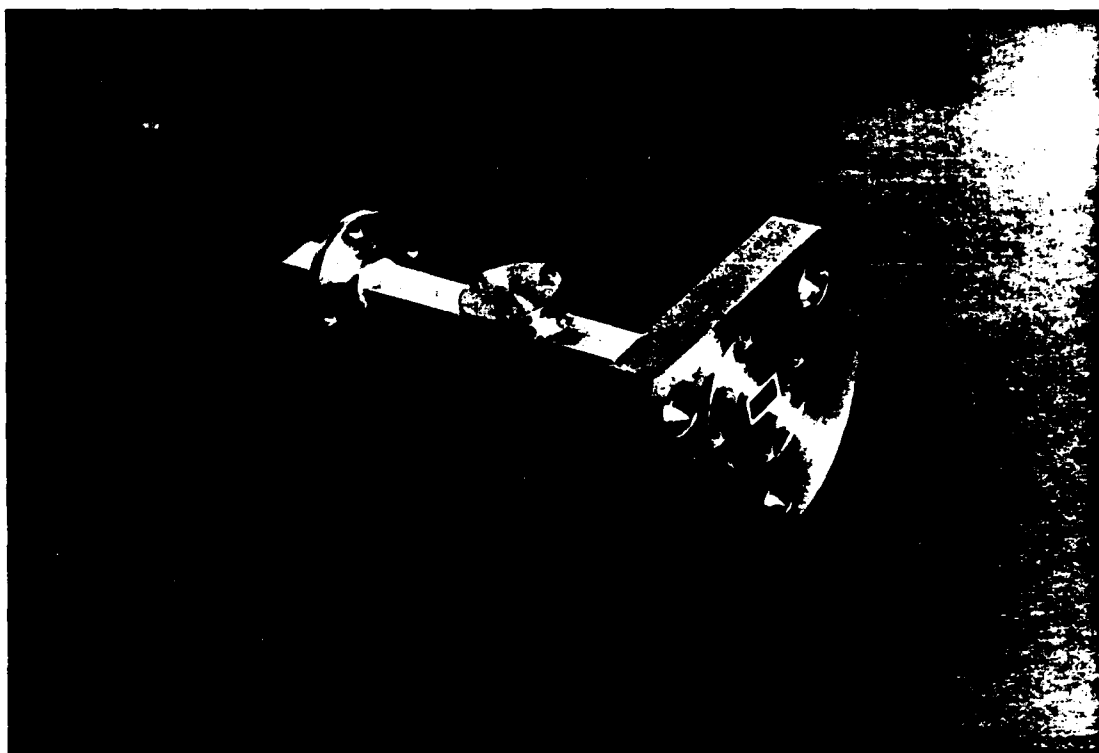
Figure 15. Tissue cell with side loading.
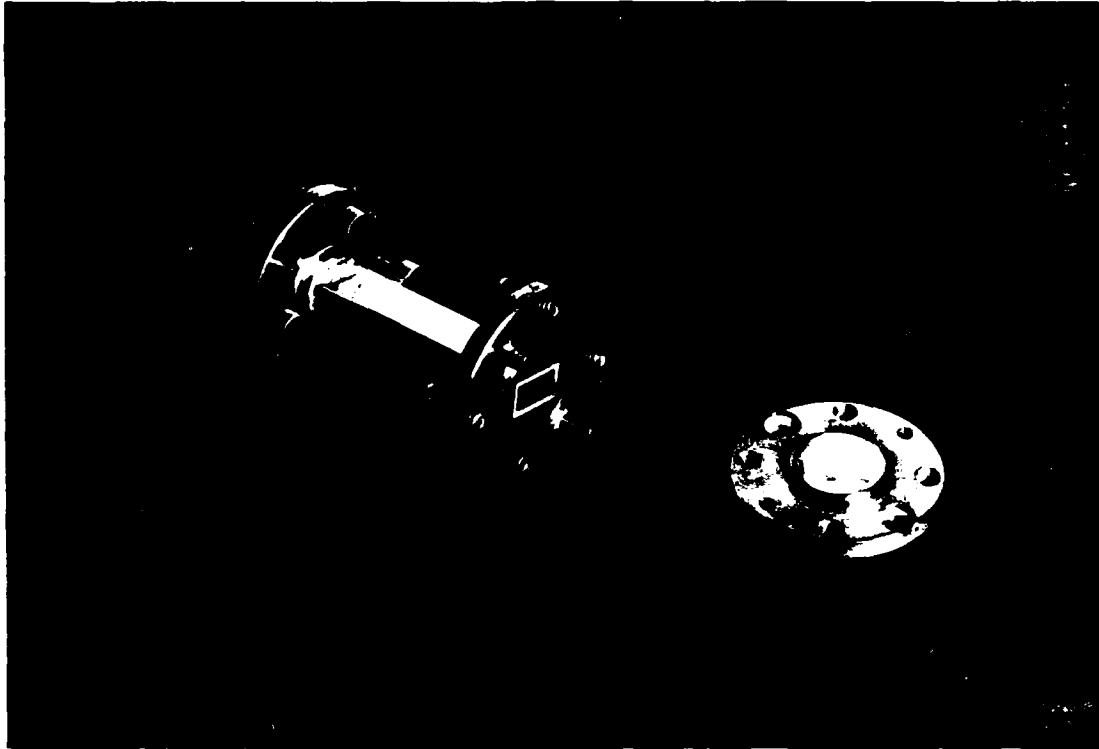
Figure 16.   The alternative tissue cell.
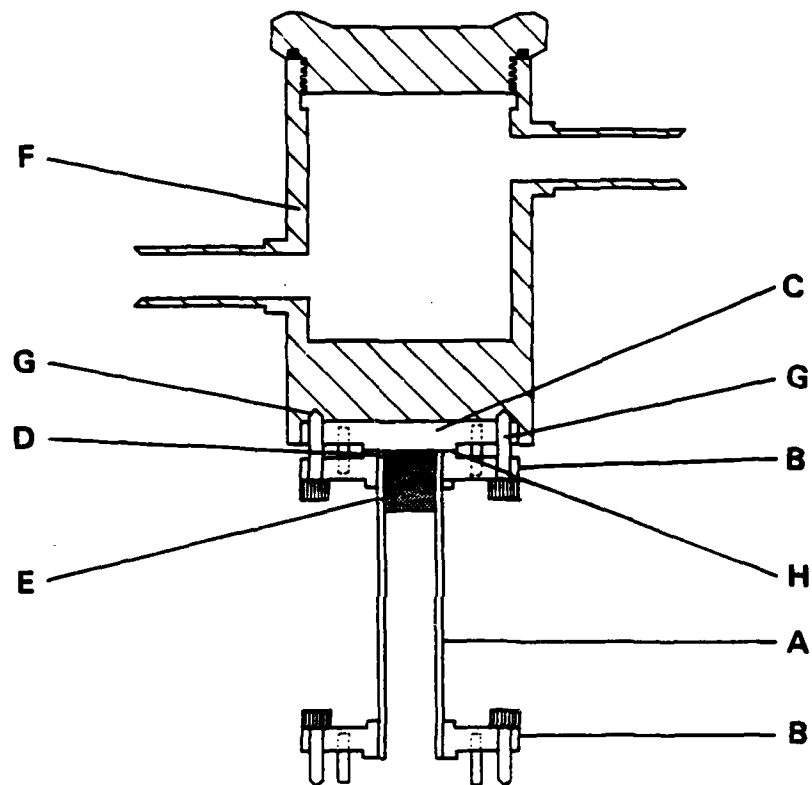
```
        5 cm
```

A. Waveguide   D. Tissue Sample   G. Screws
B. Flanges   E. PTFE Plug   H. Thermistor Probe
C. Short Circuit   F. Water Jacket

Figure 17. Cross section of alternative cell.

Figure 18. The VDU display during data acquisition.

9. PRELIMINARY RESULTS - TESTING THE SYSTEM AND CONSIDERATION OF ERRORS

A full range of experimental data are considered in Section 10; here some test data are presented and experimental errors are considered.

9.1 Cell for Liquid Samples

Results at 20°C and 25°C for distilled deionized water, ethanol (0.2% water maximum), methanol (0.1% water maximum), and fresh rabbit blood at 25°C are presented in Table 3. The blood contained a minimal amount of the anti-clotting agent heparin to maintain viability for at least 1 h at room temperature.

The errors shown are the 95% confidence intervals obtained from the least squares fitting procedure. The RMSE of fit can also give a useful indication of the reliability and stability of the system. A typical reflection profile for water would consist of about 30 data points spaced 0.06 mm apart. The average amplified detector output is around 5 to 6V, and this output leads to an RMSE which is typically between 0.001 and 0.003 V; such low values of RMSE imply that the inherent system errors are extremely low.

Apart from the statistical errors just mentioned, there are systematic errors to be considered. As mentioned previously, the frequency counter can lock the oscillator to ±1 Hz in 35 X 10^9 Hz so that frequency errors are negligible. Any uncertainty in the size of the broad dimension of the wave-guide would lead to an error in the measured complex permittivity. The short circuit was moved through the empty sample cell at three different phase locked frequencies and the guide wavelengths were measured. From these data, the broad dimension was found to be 7.092 ± 0.020 mm compared with 7.112 ± 0.020 mm given by the manufacturer. This uncertainty, coupled with a tempera-ture measurement error of 0.05°C, was estimated to lead to additional errors of 0.16% in ϵ' and 0.04% in ϵ'' for water at 20°C.

Thus, from Table 3 and the considerations just mentioned, errors in ϵ' range from 0.5% to 2.3% and those of ϵ'' range from 0.7% to 1.7%. There are no known recent data with which to compare this work. However, Grant and Shack[26] measured water at 34.86 GHz and agreed well with the present ϵ' data although their loss values at 20°C were 1.6 units higher. Saxton et al.[27] published the permittivity of alcohols at 33.16 GHz at 20°C, and their permit-tivity data for methanol and ethanol agree well with the present work although again the loss values were higher.

The just mentioned results on liquids at 35 GHz were considered highly satisfactory and suggested that the system was working well.

31

TABLE 3:   RESULTS FOR VARIOUS LIQUIDS AT 35 GHz

Liquid	Temperature/°C	ϵ'	$100(\Delta\epsilon'/\epsilon')$*	ϵ''	$100(\Delta\epsilon''/\epsilon'')$
Water	20	19.6	1.5	28.7	0.7
Water	25	22.4	1.8	30.1	0.7
Ethanol	20	3.83	0.5	1.16	0.9
Ethanol	25	3.83	0.3	1.20	1.7
Methanol	20	5.40	0.6	3.15	1.3
Methanol	25	5.41	0.6	3.28	1.2
Rabbit Blood	25	19.2	2.1	0.8	0.8

*The errors correspond to the 95% confidence intervals.

9.2   Cell for Solid Samples - Liquid Measurements

The main physical difference between solid and liquid cells is that with the former sample thickness can not be varied.   A decision was made to ini-tially test the solid cell with liquid samples to assess its performance and accuracy.

For all the measurements, a PTFE block was used to support the sample against a fixed short circuit, and to keep all of the dielectric interfaces normal to the direction of wave propagation.   The PTFE presents a minimized mismatch if half or multiple-half wavelength (in the PTFE) blocks are used. To choose the correct length of this material, the permittivity was measured using the method described by Roberts and Von Hippel.[21]   Six lengths ranging from 5 mm to 30 mm were measured, giving an average permittivity value of ϵ' = 1.988 ± 0.007.   However, to achieve a liquid-tight seal, the PTFE blocks eventually used were milled to a cross-sectional dimension slightly larger than that of the waveguide cell.   These blocks were then chilled and conse-quently shrunk before insertion into the cell.   After returning to room tem-perature, the PTFE tended to expand along the waveguide slightly, and the permittivity rose to 2.028.

For optimum accuracy, the sample under test must have a length approximately equal to one-quarter of a wavelength within the sample. For water and high water content biological tissue at 35 GHz, this length is approximately 0.50 mm. For ethanol, the length is slightly more than 1.00 mm. To achieve the required sample length, the PTFE is displaced down the guide by a metal strip having the desired thickness. Several of these strips, having various thicknesses, were made to produce sample lengths ranging from 0.4 mm to 1.2 mm.

Using the microcomputer controlled slotted line, a set of 20 equally spaced data points are automatically recorded in the standing wave pattern whose magnitude and phase are a function of the permittivity of the sample. These data points are then subsequently fitted to equation (10) in the usual way to calculate the complex permittivity of the sample.

The results for water and ethanol at 25°C are presented in Table 4; as expected the "solid" technique has larger errors than those for the liquid method presented in Table 3; however, a good agreement is obtained for the two methods. The main errors for this system are due to: (1) sample thickness, (2) PTFE thickness, (3) cut-off constant, (4) PTFE permittivity, (5) the position of the air/PTFE interface, and (6) sample temperature. Efficiency of cell packing particularly for measurements on solids is reflected in the random scatter of the data due to repeated measurement, whereas the others are not (except for (1) if several different sample lengths are used). The total system error is calculated as the sum of the squares of each component error. The dominant error is, of course, the sample thickness, but at such high frequencies the others cannot be neglected. All of these thicknesses lead to errors in the permittivity of 5.5% and 1% for water and ethanol respectively. The loss errors are far lower, being 0.7% and 0.8% for water and ethanol respectively. Thus, the total error given in Table 4 is a combination of system errors plus random scatter (95% confidence intervals) from several experiments.

However, it should be stressed that the measurements presented in Table 4 were only taken with the solid cell to investigate its behavior. If the most accurate data were required, then the liquid cell of Section 7.1 would always be used.

TABLE 4. RESULTS FOR LIQUIDS USING THE SOLID MEASUREMENT TECHNIQUE

Sample	Temperature/°C	ϵ'	$\Delta\epsilon'$	$100(\Delta\epsilon'/\epsilon')$*	ϵ''	$\Delta\epsilon''$	$100(\Delta\epsilon''/\epsilon'')$*
Water	25	21.5	1.5	7.3	29.3	0.6	2.2
Ethanol	25	3.86	0.16	4.0	1.26	0.04	3.3

*The errors correspond to 95% confidence interval.

10. EXPERIMENTAL RESULTS

10.1 Sample Preparation

Each result (presented later) is the average of repeated experiments on tissue from, typically, two white New Zealand rabbits weighing no less than 2.5 kg. This procedure prevents excessive data scatter due to significant age-related differences in water content for some tissues.[8] Muscle was excised from the hind leg of the animal where the tissue is relatively free of fat and not excessively perfused with blood. Skin samples were excised from the same region after removal of all traces of fur. The samples were scraped from the skin surface with a scalpel. Fat was taken from under the abdomen of the rabbit, and all tissues were stored under polythene sheets to prevent any moisture loss. White matter (from the brain stem) and grey matter (from the cerebral cortex) were loaded into syringes immediately after excision. All measurements reported were performed within 24 h of animal death (CO_2 overdose).

For brain tissue and eye lens, the samples were syringed on to the recessed PTFE window in the waveguide cell. Excess tissue was squeezed out between the short circuit and the waveguide aperture as the short circuit was firmly screwed into position. Sample temperature was controlled to within 0.5°C by a small water jacket situated in contact above the short circuit and was monitored by a thermistor probe next to the guide aperture.

Muscle, skin, and fat samples were impossible to load in this fashion because of the mechanical properties of the tissues. Another method was devised to produce a sample having the same cross-sectional dimension of the guide, in addition to having almost the correct thickness. First, the tissue was cut into a long strip and pushed into a length of waveguide against a PTFE block. A small rectangular rod was then used to gently compress the tissue, causing it to properly fill the guide. The next stage involved freezing the

tissue inside the guide, in the ice-making compartment of a domestic refrig-
erator. This step usually took 2 to 3 minutes to complete. The tissue was
then pushed out of the guide as a solid block and sliced with a chilled cut-
ting tool. This tool consisted of two conventional razor blades separated by
a thin metal strip between the center and upper edges, such that the sliced
sample would be slightly greater (i.e., approximately 0.05 mm) than the
required thickness. Still frozen, the sample was positioned in the cell, and
the short circuit firmly affixed. The PTFE windows used for these experiments
were made to slip down the guide under a moderate pressure to allow the thaw-
ing sample to expand down the length of the guide slightly, precluding any
significant compression. Thus, after an experiment, the short circuit and
sample were removed enabling the sample gap to be remeasured before the data
analysis. Typically, this gap may increase in size by between 0.05-0.10 mm
before the thermostated sample is actually measured.

At low temperatures, the fat samples could not be frozen but became wax-
like. In this state, the samples were suitable for slicing. Owing to the low
permittivity and dielectric loss of fat by comparison with the other tissues
considered, it was necessary to increase the optimum sample thickness from
approximately 0.50 mm to 1.00 mm.

10.2   Dielectric Properties of Rabbit Tissue at 35 GHz

Using the experimental system and cell described in Sections 6 and 7.2,
the complex permittivity of various rabbit tissues was measured at 35 GHz,
mainly at temperatures of 20 and 37°C. The results for muscle, fat, and skin
are presented in Table 5; the conductivity and the attenuation coefficient
have also been calculated. As expected, the permittivity and loss of muscle
and fat are relatively high (ϵ' = 3.6 and ϵ'' = 1.4 at 37°C). In Table 6, the
corresponding results are shown for grey matter and white matter. Again, the
permittivity and loss are high although the loss for white matter is less than
grey matter (ϵ'' = 14.4 for white against 20.0 for grey at 37°C). In Table 7,
data are presented for rabbit lens cortex and rabbit lens nucleus. Although
the lens cortex has a high permittivity and loss (ϵ' = 14.5, ϵ'' = 17.4 at
20°C), the values for lens nucleus are much lower (ϵ' = ϵ'' = 8.9 at 23°C).

To consider one of the high loss tissues, for example, brain grey matter
at 37°C, it can be seen from Table 6 that the conductivity and electric field
attenuation coefficients are 38.9 $S \cdot m^{-1}$ and 12.7 $dB \cdot mm^{-1}$. By comparison, at
2.45 GHz, these quantities are only 1.7 $S \cdot m^{-1}$ and 0.4 $dB \cdot mm^{-1}$ reflecting a
large loss at the higher frequency due to dipolar reorientation of bulk water
molecules within the tissue. This comparison is a property of all the high
water content tissues which includes skin, muscle, brain, and the eye lens.
Consequently, the depth of penetration is low in each case. For example, the
field propagation through skin should fall to (1/e) of its initial value

after only 0.7 mm. In contrast, for rabbit fat, the corresponding distance is approximately 3.8 mm, due to the far lower attenuation coefficient for this particular tissue.

In recent publications,[7,9] the dielectric properties of rabbit brain and eye lens were reported in the frequency range 1 to 18 GHz; this work forms part of the previous project for AFOSR. For each tissue, the experimental data were adequately described by the Cole-Cole function,

$$\epsilon = \frac{\epsilon_s - \epsilon_\infty}{1 + (jf/f_R)^{1-\alpha}} + \epsilon_\infty \frac{j\sigma_i}{2\pi f \epsilon_0} \qquad (15)$$

where all the symbols have their usual meanings. The fitted parameters (i.e., ϵ_s, ϵ_∞, f_R, and σ_i) are now used to generate values of permittivity and dielectric loss at 35 GHz for grey matter, white matter, and lens cortex at 37°C and 20°C. In Table 8, a comparison of these with the experimental data is given. As expected, it is not possible to resolve significant differences between the generated and experimental data for each tissue. However, this comparison shows the validity of the Cole-Cole model for predicting the complex permittivity for brain and lens tissue at 35 GHz.

This conclusion is important since, if the tissues showed any anomalous behavior at 35 GHz, then the experimental results would be expected to differ significantly from those predicted by the Cole-Cole equation by lower frequency data. As mentioned in Section 2, it was not a prime objective of this work to look for resonances; to do so properly would require a frequency variation. The agreement between the experimental and the predicted does suggest that the dielectric behavior is not anomalous at this frequency.

To complete the rabbit study, blood was measured at 25 and 37°C; the results are presented in Table 9. Both ϵ' and the loss are higher than for the rabbit tissues, the values being $\epsilon' = 23.6$ and $\epsilon'' = 25.6$ at 37°C.

In Figure 19, the rabbit data at 37°C are shown as a plot of ϵ' against ϵ'' to give a visual indication of the spread of some key tissues.

TABLE 5. RESULTS FOR RABBIT MUSCLE FAT AND SKIN AT 35 GHz

Tissue	Temp/°C	No. of Rabbits	No. of Experiments	ϵ'	ϵ''	$\sigma/S\ m^{-1}$	$\alpha/dB\ mm^{-1}$
Muscle	37	2	12	19.1 ±1.5	20.5 ±1.8	39.9	13.5
	20	2	13	15.3 ±1.3	17.9 ±0.8	34.9	12.9
Fat	37	2	10	3.6 ±0.3	1.4 ±0.4	2.7	2.3
	20	1	4	3.4 ±0.3	1.3 ±0.6	2.5	2.2
Skin	32.5	2	9	17.3 ±1.2	19.2 ±1.3	37.4	13.2

TABLE 6. RABBIT BRAIN TISSUES AT 35 GHz

Tissue	Temp/°C	No. of Rabbits	No. of Experiments	ϵ'	ϵ''	$\sigma/S\ m^{-1}$	$\alpha/dB\ mm^{-1}$
Grey Matter	37	2	13	21.3 ±0.9	20.0 ±0.8	38.9	12.7
	20	2	11	17.0 ±0.9	18.6 ±1.0	36.2	12.9
White Matter	37	2	10	17.8 ±1.7	14.4 ±1.3	28.0	10.2
	20	2	8	14.9 ±1.0	14.3 ±1.3	27.8	10.8

TABLE 7. RESULTS FOR RABBIT LENS AT 35 GHz

Tissue	Temp/°C	No. of Rabbits	No. of Experiments	ϵ'	ϵ''	$\sigma/S\ m^{-1}$	$\alpha/dB\ mm^{-1}$
Lens Cortex	37	2	7	17.9 ±1.4	19.8 ±1.9	38.6	13.4
	20	2	8	14.5 ±0.8	17.4 ±2.2	33.9	12.9
Lens Nucleus	23	3	3	8.9 ±0.4	8.9 ±0.5	17.3	8.7

TABLE 8. THE EXPERIMENTAL RESULTS AT 35 GHz COMPARED WITH DATA PREDICTED USING THE COLE-COLE MODEL FROM RESULTS TAKEN BETWEEN 1 AND 18 GHz

Tissue	T/°C	Predicted From Cole-Cole Fits of 1-18 GHz Data		Experimental Values	
		ϵ'	ϵ''	ϵ'	ϵ''
Grey Matter	20	16.0 ± 1.3	17.0 ± 0.8	17.0 ± 0.9	18.6 ± 1.0
	37	20.5 ± 1.2	18.7 ± 0.9	21.3 ± 0.9	20.0 ± 0.8
White Matter	20	14.0 ± 1.1	12.6 ± 0.7	14.9 ± 1.0	14.3 ± 1.3
	37	16.6 ± 1.4	13.5 ± 1.5	17.8 ± 1.7	14.4 ± 1.3
Lens Cortex	20	13.4 ± 1.3	15.7 ± 0.7	14.5 ± 0.8	17.4 ± 2.2
	37	18.6 ± 1.1	17.4 ± 0.8	17.9 ± 1.4	19.8 ± 1.9

10.3   Phantom Tissue Equivalents

In addition to the measurements of fresh rabbit tissue, various mixtures of water and ethanediol, water and ethanol, and water and glycerol were examined to find suitable tissue-equivalent materials (phantoms). These mixtures at ambient temperature 25°C ought to reflect the dielectric properties at around 32-33°C. Most of the tissues listed in Tables 5 to 8 have a complex dielectric constant of approximately (19-j20) at 37°C. For a water-based mixture to simulate these properties at 25°C, it is necessary to first consider the dielectric properties of water at two temperatures. The complex permittivity is (22.4 - j30.1) at 25°C and 37°C respectively. At 35 GHz, liquids such as alcohols and diols reduce the volume occupied by water molecules, and as a result the complex permittivity is lowered. For the concentration of mixtures examined in the present work, permittivity and loss were found to be lowered in roughly the same proportion. However, the reduction was required to lower the permittivity from 22.4 units to approximately 19 units (15% reduction). The corresponding reduction in dielectric loss, 29.8 units to around 20 units would be around 33%. Hence, for the mixtures described at 25°C, it was not possible to match both the permittivity and dielectric loss for any mixture. For example, by matching permittivity at the appropriate value (i.e., varying the concentration of the mixture), the loss would be too high to simulate a tissue at 37°C. Therefore, a "compromise" mixture, having a slightly lower permittivity and a higher dielectric loss (at 25°C) than a typical issue at 37°C, was chosen to be the most suitable.

Since the permittivity of fat is low by comparison to the other tissues considered, mixtures of the kind just described are unsuitable. However, the complex permittivity and loss of the pure ethanol at 25°C (3.82 - j1.2) is similar to the corresponding value for fat (3.6 - j1.4) at 37°C. This result, with the other phantom recipe, is given in Table 10.

10.4   Pure Water and Saline

Because of the importance of water in biological systems, accurate data on its electrical properties at 35 GHz over a temperature range would be useful. The data were obtained using the liquid cell described in Section 7.1. The results for a temperature range of 20 to 37°C are presented in Table 11 and Figures 20 and 21. The errors quoted in Table 11 are the 95% confidence intervals and are about 0.35 units in ϵ' and 0.3 units in ϵ''.

Measurements were also made on saline and the results obtained at a concentration of 0.95% NaCl at 20 and 37°C are presented in Table 12. As expected, the errors are of the same order as for water.

TABLE 9.   RESULTS FOR RABBIT BLOOD AT 35 GHz

Temp/°C	No. of Rabbits	No. of Experiments	ϵ'	ϵ''	$\sigma S\ m^{-1}$	$\alpha/d\ mm^{-1}$
25	1	6	19.2 ± 0.4	24.8 ± 0.2	48.3	15.7
37	2	8	23.6 ± 0.3	25.6 ± 0.2	49.8	15.1

TABLE 10.   TISSUE-EQUIVALENT MATERIALS AT 25°C, 35 GHz

Composition By Weight	Simulating:-	ϵ'	ϵ''	$\alpha/dB\ mm^{-1}$
14.4% Ethanediol	High Water Content Tissue	15.7	22.9	15.65
85.96% Water				
Pure Ethanol	Fat	3.82	1.20	1.93
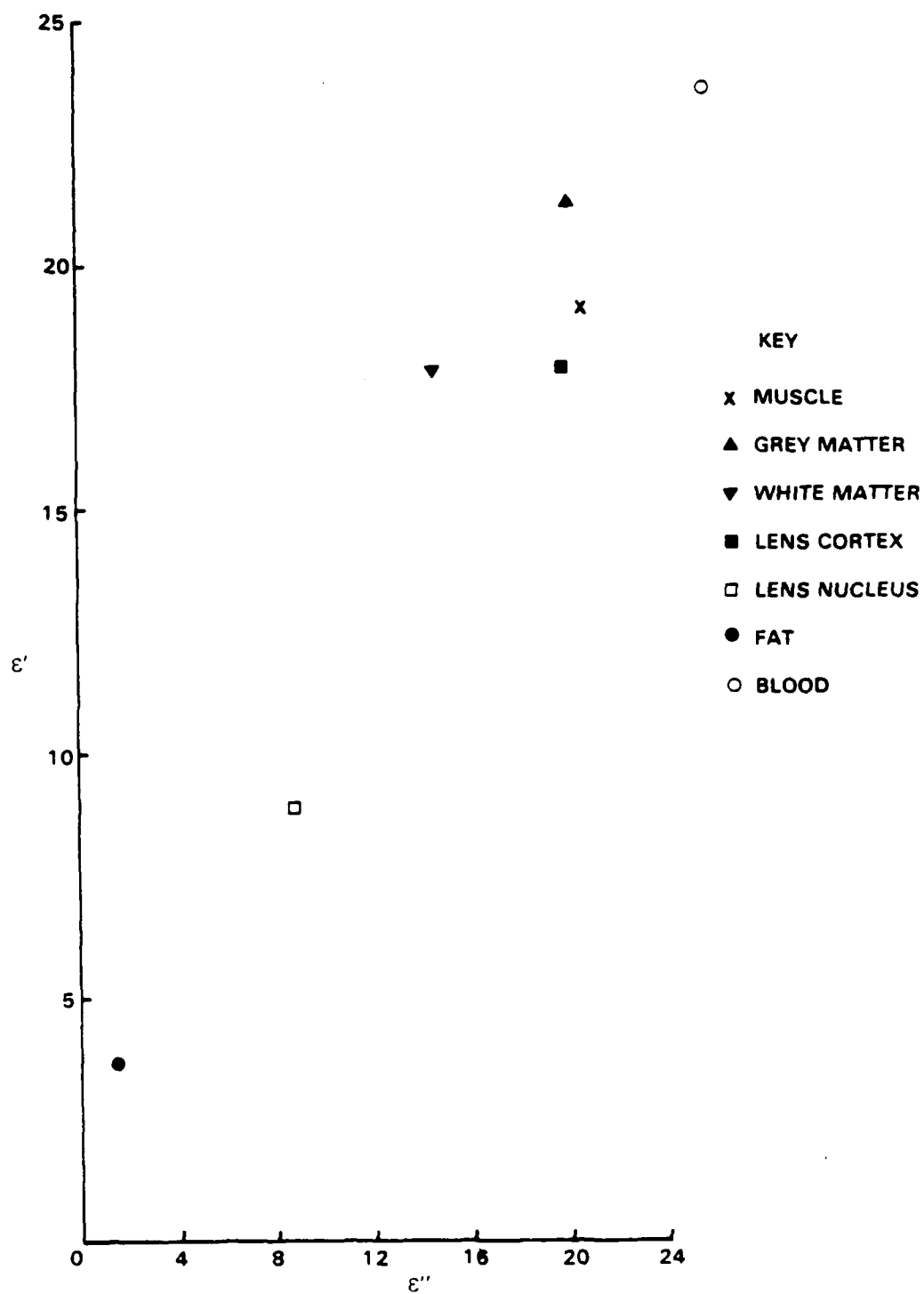
Figure 19. ε' against ε" for rabbit tissues at 35 GHz, 37°C.

TABLE 11. RESULTS FOR PURE WATER AT 35 GHz

Temp/°C	ϵ'	ϵ''
20	19.6 ± 0.3	28.7 ± 0.2
22	20.6 ± 0.2	29.2 ± 0.3
24	21.7 ± 0.3	29.8 ± 0.2
25	22.4 ± 0.4	30.1 ± 0.2
26	22.9 ± 0.3	30.4 ± 0.2
28	23.9 ± 0.2	30.8 ± 0.2
30	25.1 ± 0.3	31.4 ± 0.3
32	25.9 ± 0.5	31.8 ± 0.5
34	26.9 ± 0.5	31.9 ± 0.5
36	27.9 ± 0.5	32.3 ± 0.5
37	28.7 ± 0.3	32.7 ± 0.5

TABLE 12. RESULTS FOR SALINE (0.95% NaCl) AT 35 GHz

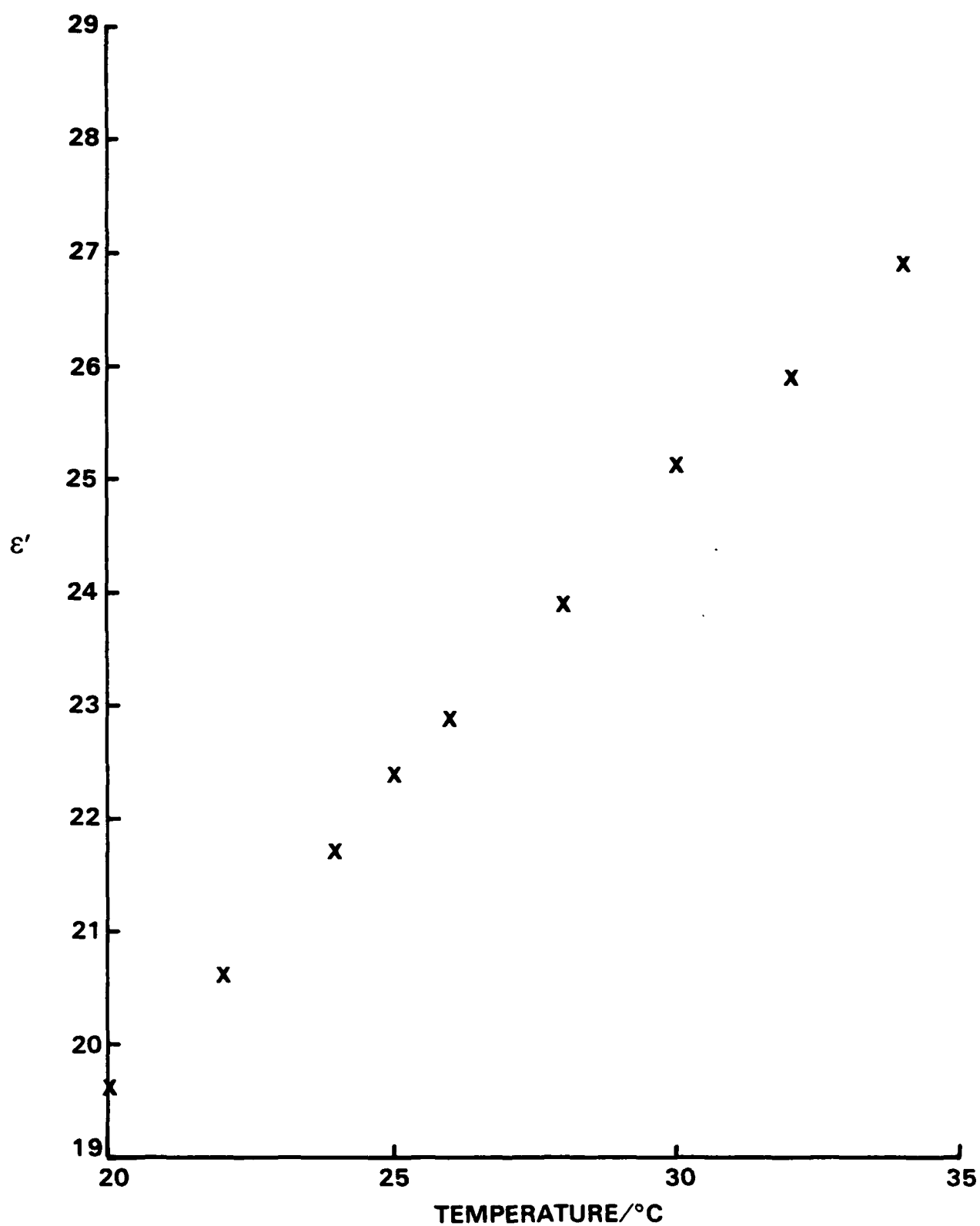| Temp/°C	ϵ'	ϵ''
20	19.9 ± 0.4	28.7 ± 0.2
37	28.8 ± 0.3	32.2 ± 0.2

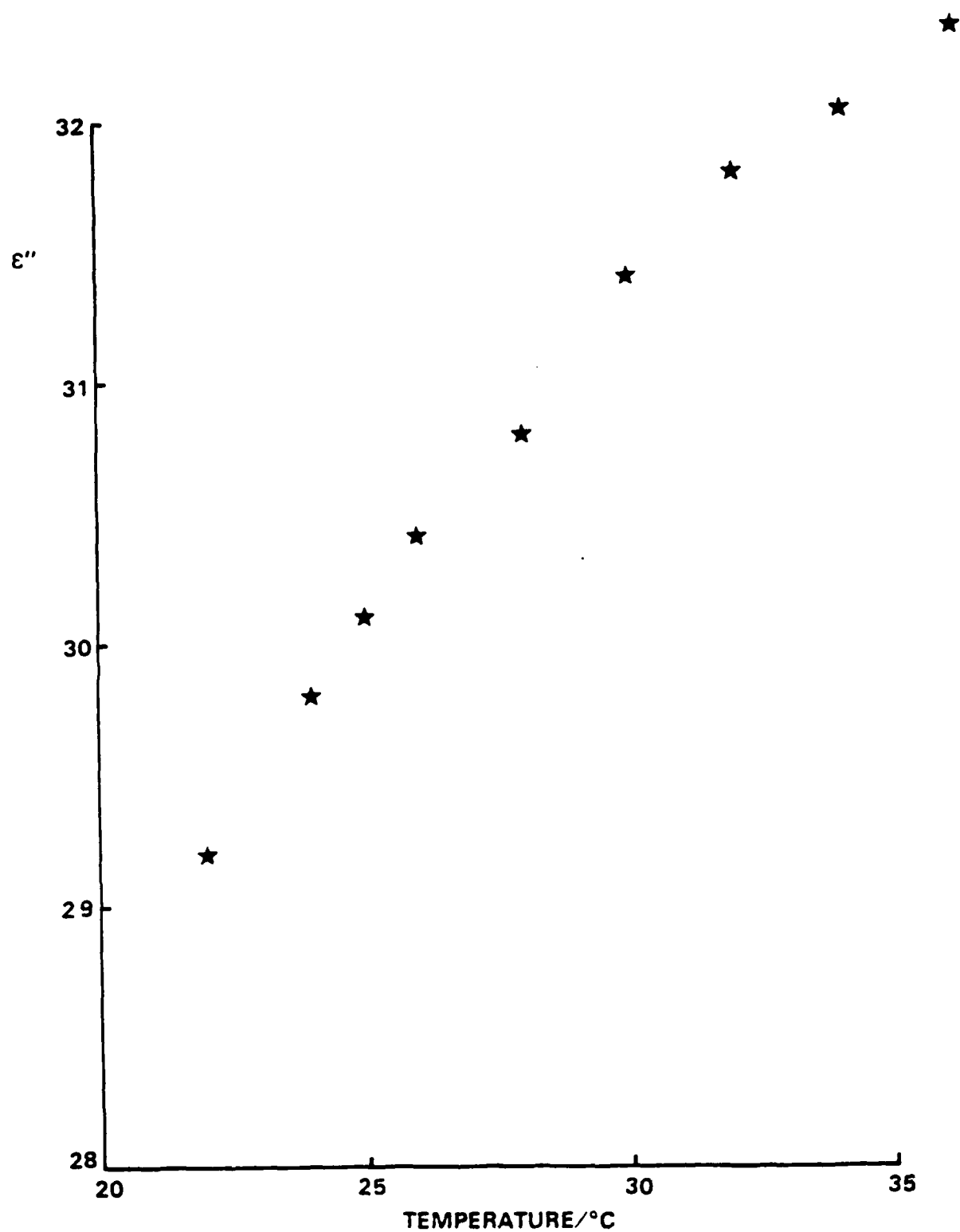Figure 20.   ε' against temperature for water at 35 GHz.

Figure 21. ε" against temperature for water at 35 GHz.

10.5 Analysis of the Water Data

Although the dielectric behavior of water has been well documented over the years, there is still some uncertainty regarding the relaxation mechanism(s). In particular, many workers have reported that water displays a small distribution of relaxation frequencies, characterized by the Cole-Cole alpha parameter. One aim of the present work was to combine the data for water at 35 GHz with the recent low-frequency data (1 to 15 GHz of Nightingale[28] to fit them to equation 15.

The results of this analysis for water at 20°C, 25°C, and 30°C are given in Table 13. The parameter ϵ_s was held constant in each case at the value given by Malmberg and Maryott.[30] The parameters varied were ϵ_∞, f_R, and α. For the Debye properties, α was held constant at zero. The results show clearly for the three temperatures, α is not significantly different from zero, despite the low overall error in this parameter. Also, ϵ_∞ has not altered significantly over this 10°C temperature range.

TABLE 13. AN ANALYSIS OF WATER DATA AT 35 GHz BETWEEN 20 AND 30°C

Temp	ϵ_s	ϵ_{inf}	f_R/GHz	α	RMSE
20	80.10	5.72 ± 0.28	16.77 ± 0.09	-	0.2190
	80.10	5.74 ± 0.33	16.76 ± 0.13	-0.0004 ± 0.003	0.2188
25	78.30	5.55 ± 0.42	19.17 ± 0.16	-	0.2702
	78.30	5.75 ± 0.46	19.05 ± 0.21	-0.0034 ± 0.004	0.2589
30	76.54	5.45 ± 0.55	21.56 ± 0.23	-	0.3295
		5.44 ± 0.58	21.57 ± 0.25	0.0001 ± 0.003	0.3295

REFERENCES

1. Schwan, H. P. Electrical properties of tissues and cells. In Biol Med Phys 5: Academic Press, 1957

2. Thurai, M., et al. Variation with age of the dielectric properties of mouse brain cerebrum. Phys Med Biol 29:1133-1136 (1984).

3. Gabriel, C., et al. Dielectric properties of ocular tissues at 37°C. Phys Med Biol 28:43-49 (1983).

4. Foster, K. R., et al. Microwave dielectric relaxation in muscle: a second look. Biophys J 29:271-281 (1980).

5. Stuchly, M.A., et al. Measurement of radiofrequency permittivity of biological tissue with an open ended coaxial line: Part II experimental parts. Trans IEEE MTT-30:87-92 (1982).

6. Steel, M., et al. A precision method for measuring the complex permittivity of solid tissue in the frequency domain between 2 and 18 GHz. J Phys E 17:30-34 (1984).

7. Steel, M. C., and Sheppard, R. J. Dielectric properties of mammalian brain tissue between 1 and 18 GHz. Phys Med Biol 30:621-630 (1985).

8. Thurai, M., et al. Dielectric properties of developing rabbit brain at 37°C. Bioelectromagnetics 6:235-242 (1985).

9. Steel, M. C., and Sheppard, R. J. Dielectric properties of lens tissues at microwave frequencies. Bioelectromagnetics 7:73-81 (1986).

10. Gandhi, O. P., et al. Millimetre wave absorption spectra of biological samples. Bioelectromagnetics 1:285-298 (1980).

11. Ghodgaonkar, D. K., et al. Complex permittivity measurements of biological tissues and human skin in-vivo at millimeter wavelengths. Paper presented at the 7th Annual meeting of the Bioelectromagnetics Society (BEMS), 1985.

12. Crowgey, S. R., et al. Effects of High Power Millimeter Waves. Report submitted to the Air Force School of Aerospace Medicine under contract F 334615-83-D-0601, 1984.

13. Edrich, J., and Hardee, P. Complex permittivity and penetration depth of muscle and fat tissue between 40 and 90 GHz. Trans IEEE MTT-24:273-275 (1976).

14. Frohlich, H. Coherent electric vibrations in biological systems and the cancer problem. Trans IEEE MTT-26:613-617 (1978).

15. Frohlich, H. The biological effects of microwaves and related questions. In Advances in Electronics & Electron Physics 53:85-152 (1980).

16. Grundler, W., and Keilmann, F. Non-thermal effects of microwaves on yeast growth. Z Naturforsh 33c:15-22 (1978).

17. Grundler, W. Recent results of experiments on non-thermal effects of millimetre microwaves on yeast growth. Collective Phenomena 3:181-186 (1981).

18. Edwards, G. S., et al. Resonant microwave absorption of selected DNA molecules. Phys Rev Letts 53:1284-1287 (1984).

19. Furia, L., et al. Do millimetre waves affect yeast growth rate? Paper presented at the 7th Annual meeting of the Bioelectromagnetics Society (BEMS), 1985.

20. Grant, E. H. Accurate determination of the permittivity and conductivity of biological tissue at centimetre and millimetre wavelengths. USAFSAM-TR-84-33, Apr 1984.

21. Roberts, S., and Von Hippel, A. A new method for measuring the dielectric constant and loss in the range of centimetre waves. J Appl Phys 17:789-796 (1946).

22. Nightingale, N. R. V. Ph.D. Thesis: University of London, 1981.

23. Szwarnowski, S., and Sheppard, R. J. Precision waveguide cells for the measurement of permittivity of lossy liquids at 70 GHz. J Phys E 10:1163-1167 (1977).

24. Sheppard, R. J. Accurate determination of the complex permittivity of biological tissue around 35 GHz. Preliminary report to AFOSR for the period 15 Mar 84 to 14 Mar 85 (1985).

25. Sheppard, R. J. The least squares analysis of complex weighted data with dielectric applications. J Phys D 6:790-794 (1973).

26. Grant, E. H., and Shack, R. Complex permittivity measurements at 8.6 mm wavelength over the temperature range 1-60°C. Brit J Appl Phys 18:1807 (1967).

27. Saxton, J.A., et al. Dispersion at millimetre wavelengths in methyl and ethyl alcohols. J Chem Phys 37:2132-2139 (1962).

28. Szwarnowski, S. Apparatus and techniques for measuring the permittivity of water and lossy liquids at 70 GHz. Ph.D. Thesis: University of London, 1979.

29. Nightingale, N. R. V., et al. A coaxial line cell for measuring the permittivity of medium to high loss liquids in the frequency range 2 to 15 GHz. J Phys E 14:156-160 (1981).

30. Malmberg, C. G., and Maryott, A. A. J Res Natl Bur Stand (US) :60-609 (1956).